UNIVERSITÀ DI PARMA

UNIVERSITA' DEGLI STUDI DI PARMA

DOTTORATO DI RICERCA IN
"MEDICINA MOLECOLARE"
CICLOXXXIII

EFFECTS OF IN VIVO GREEN TEA EXTRACT ADMINISTRATION ON CONTRACTILE PERFORMANCE AND MITHOCONDRIAL FUNCTION OF VENTRICULAR CARDIOMYOCYTES, IN HEALTY AND DIABETIC RATS.

Coordinatore:

Chiar.mo Prof. Prisco Mirandola

Tutore:

Chiar.ma Prof.ssa Donatella Stilli

Co-Tutori:

Chiar.ma Prof.ssa Monia Savi

Chiar.ma Prof.ssa Federica Maria Angela Rizzi

Dottoranda**: Rocchina Vilella**

Anni Accademici 2017/2018 – 2019/2020

Index

1. INTRODUCTION

1.1 Polyphenols and health effects

Polyphenols, a heterogeneous group of molecules, are the most abundant secondary metabolites of plants. Physiologically, these molecules are produced to defence the plants against environmental stressors, such as ultraviolet lights, free radicals, and uncommon temperatures, as well as contributing to the colour of leaves, berries and fruits [Kabera JN, 2014].

More than 8000 different polyphenols have been identified, each one with specific properties and bioavailability [Finicelli M, 2019]. They can be classified into different groups based on the number of phenol rings contained and structural elements that bind these rings to one another. Distinctions are thus made between the phenolic acids, flavonoids, stilbenes, and lignans (*figure 1*)[Manach C, 2004].

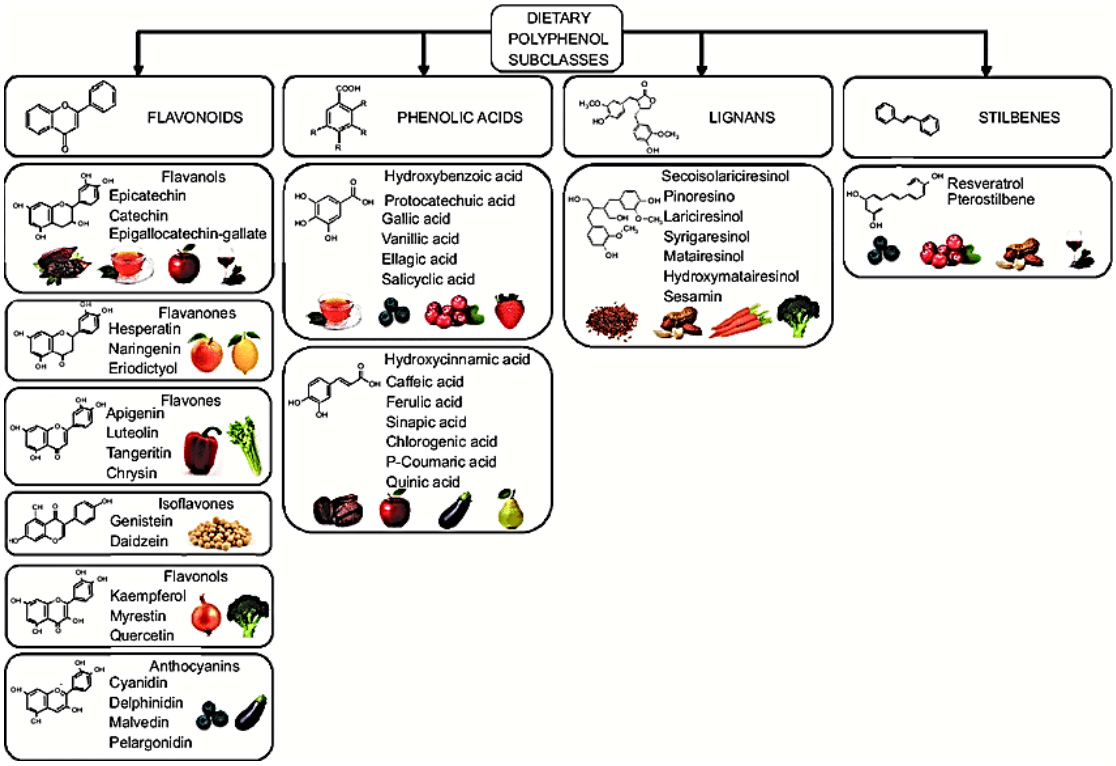

Figure 1. Dietary polyphenol subclasses, their basic chemical structure and typical dietary sources [Woodward KA, 2018].

A huge body of literature highlights polyphenol beneficial effects on human health due to their antioxidant and anti-inflammatory properties. Consumption of foods rich in phenolic compounds as high as 1 g per day is considered safe and beneficial for chronic disease prevention [Zhang H, 2016]. Epidemiological, clinical and nutritional studies strongly support the evidence that dietary phenolic compounds enhance human health

by lowering risk and preventing the onset of degenerative diseases including cancers, cardiovascular diseases and metabolic disorders [Finicelli M, 2019].

The health effects of polyphenols depend on the amount consumed and their bioavailability [Manach C, 2004]. Indeed, not all polyphenols are absorbed with equal efficacy because they are extensively metabolized by intestinal and hepatic enzymes and intestinal microflora. Additionally, variability in human microbiota might be responsible for the differences observed in the metabolism of polyphenols, thus influencing or varying their bioactive properties [Nicholson JK, 2012; Amiot MJ, 2016].

As a consequence, a deeper knowledge of the bioavailability and metabolism of polyphenols is necessary to evaluate their biological activity within target tissues [Manach C, 2004].

A wide range of pharmacological activities, including antioxidant, antibacterial, hepatoprotective, anti-inflammatory, and antihyperlipidemic effects, are attributed to flavonoids [Farhat G, 2017; Bernatoniene J, 2018; Farhadi F, 2018; Rasouli H, 2018; Tungmunnithum D, 2018]. They are also known for their capacity to modulate key cellular enzyme functions such as xanthine oxidase (XO), cyclo-oxygenase (COX), lipoxygenase (LOX) and phosphoinositide 3-kinase (PI3K), and cellular signalling pathways [Metodiewa D, 1997; Walker EH, 2000].

Flavonoids are the most common polyphenols in human diets. They are abundantly found in foods and beverages of plant origin, such as fruits, vegetables, grains, roots, tea, cocoa, and wine [Manach C, 2004]. Despite their abundance (more than 4,000 varieties have been described), they share a common chemical structure consisting of two aromatic rings that are bound together by three carbon atoms to form an oxygenated heterocycle [Finicelli M, 2019].

On the basis of the type of heterocycle involved, they are further divided into six subclasses: flavonols, flavones, flavanones, flavanols (the monomer form, catechins, and polymer form, proanthocyanidins), anthocyanins, and isoflavones [Panche AN, 2016].

Specifically, flavanols are the most ubiquitous flavonoids in foods including onions, curly kale, leeks, broccoli, blueberries, red wine and tea [Manach C, 2004]. Green tea, in particular, is the richest source of catechins which have been related to the beneficial health effects of tea [Zhang H, 2014].

1.2 Tea: main features and classification

Tea is the second most popular beverage in the world behind water. It was discovered in China, where it has been used for 4000 years as a daily beverage known to have beneficial effects on health [Botten D, 2015].

All types of teas are manufactured from the same plant species, *Camellia sinensis* which belongs to the family of *Theaceae*. The plant is currently cultivated in many countries, including India, Turkey, Sri Lanka, Kenya, and others. Over the past 30 years or more, scientists have studied this plant in respect to potential health benefits [Lau SO, 2016].

The various kinds of tea, produced through different processes, can be classified into three major types: green tea (unfermented), oolong tea (semifermented), and black tea (fully fermented, *figure 2*) [Banerjee S, 2015].

Figure 2. Different kinds of tea and their manufacture.

Green tea, which makes up around 20% of tea production worldwide, is made by steaming the fresh leaves at high temperature to inactivating the polyphenol oxidases, thereby preventing the enzymatic oxidation of catechins and maintaining the monomeric forms of polyphenols [Roshanak S, 2016].

It differs significantly from black tea, primarily in terms of fermentation and oxidation process as well as the chemical composition [Armoskaite V, 2011]. Tea leaves are allowed to ferment for several hours before being either smoke fired, flame fired or steamed to make black tea. The black tea fermentation process results in the oxidation

of simple polyphenols, i.e. tea catechins, to more complex condensed molecules such as theaflavin which give black tea its typical colour and strong, astringent flavour. Oolong tea is prepared by firing the leaves shortly after rolling, and then drying the leaves. The oxidation is ended by the firing process, hence oolong tea is called semi-fermented tea. Therefore, the characteristics of oolong tea are between black and green tea [Wang H, 2000].

The lack of fermentation process of tea leaves during production preserves green tea polyphenol content, especially catechins. Green tea is widely considered as a health promoting beverage due to the presence of high levels of catechins [Gupta DA, 2014].

1.3 Green tea composition

The chemical composition of green tea is quite complex and includes more than ten groups of compounds (*figure 3*).

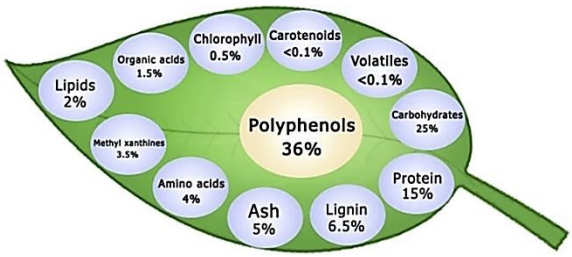

Figure 3. Chemical constituents of green tea leaves (% of dried leaf) [Al Hrooba AM, 2019].

Green tea contains proteins (15–20%), whose enzymes constitute an important fraction and amino acids (1-4% dry weight) such as theanine, 5-N-ethylglutamine, glutamic acid, tryptophan, glycine, serine, aspartic acid, tyrosine, valine, leucine, threonine, arginine, and lysine. It also contains minerals and trace elements (5% dry weight) such as calcium, magnesium, chromium, manganese, zinc, sodium, phosphorus, cobalt, strontium, nickel, potassium, and carbohydrates (5-7% dry weight) such as glucose, cellulose and sucrose. In addition, green tea is rich in sterols and lipids (linoleic and α-linolenic acids), vitamins (B, C, E), xanthic bases (caffeine, theophylline), pigments (chlorophyll, carotenoids), and volatile compounds (aldehydes, alcohols, esters, lactones, hydrocarbons) [Graham HN, 1992; Ye Y, 2018].

Furthermore, the predominant and medically relevant active components of green tea are polyphenols, which include flavanols, flavonoids, and phenolic acids. Most of the green tea polyphenols are flavanols, commonly known as catechins (flavan-3-ols), which

account for 80–90% of total flavonoids and approximately 40% of the water-soluble solids in green tea [Reygaert WC, 2017].

There are four main types of green tea catechins (GTCs): epigallocatechin-3-gallate (EGCG, 60% of green tea catechins content), epigallocatechin (EGC, 19%), epicatechin-3-gallate (ECG, 13.6%) and epicatechin (EC, 6.4%) (*figure 4*). The presence of numerous hydroxyl groups and their distribution in the molecules gives them strong antioxidant properties [Al Hrooba AM, 2019].

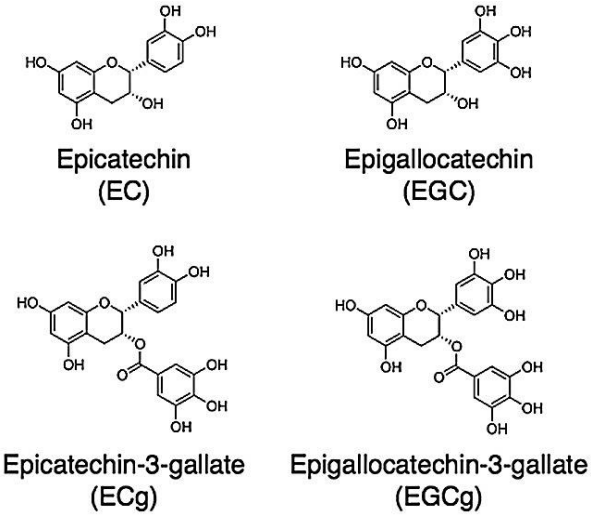

Figure 4. Chemical structure of green tea catechins.

The relative catechins content of green tea is not constant, but depends on the different processing of leaves before drying and environmental factors including geographical location, climatic and growing conditions [Zhang C, 2018].

1.4 Health benefits of green tea

Green tea has been considered by the traditional Chinese medicine as a healthy beverage since ancient times. The association between green tea consumption and human health has long been highlighted [Cabrera C, 2006].

Green tea leaves contain three main components which act upon human health: xanthic bases, e.g. caffeine that acts on central nervous system stimulating wakefulness, facilitating ideas association, and decreasing the sensation of fatigue, essential oils that facilitate digestion, and polyphenolic compounds. However, the health-promoting effects of green tea are mainly attributed to its polyphenol content [Cabrera C, 2006].

Over the past 15–20 years, a number of studies have revealed that green tea catechins, particularly EGCG, have positive biological activities. Other than antioxidant and anti-inflammatory activity, they have been found to have anticancer and antimicrobial properties [Afzal M, 2015]. Green tea and EGCG have also been shown to be involved in the regulation of a variety of metabolic processes such as hypercholesterolemia, hyperglycemia, and improving glucose tolerance in diabetes [Yousaf S, 2014; Zuo X, 2014]. Studies using *in vitro* and animal models have shown that green tea catechins provide protection against neurodegenerative diseases like Parkinson and Alzheimer [Zhang Z, 2015, Srinivasan M, 2015]. Some epidemiological, clinical, and experimental studies have also established a positive relationship between green tea catechins intake and reduced cardiovascular disorders [Bhardwaj P, 2013].

GTCs may interact with molecular targets such as proteins and phospholipids, regulate signal transduction pathways and modulate enzymes, and have a strong affinity with lipid bilayers. Cellular uptake of catechins occurs mainly by passive transport [Botten D, 2015].

However, the potential health effects of catechins depend not only on the amount consumed but also on their bioavailability after consumption [Krupkova O, 2016]. After drinking tea only a small fraction of tea catechins present in the intestinal tract can be absorbed, and then considered to be bioavailable, i.e., finding them in the blood and tissues or reaching the systemic circulation [Cai ZY, 2018].

A number of studies have been conducted to assess the bioavailability of green tea components. These studies have shown that EGCG, ECG, and EGC and EC metabolites can be detected and measured in blood plasma while only EGC and EC metabolites can be detected and measured in urine. Additionally, catechin peak concentration in blood plasma and urine occur at roughly 2 hours and between 4-6 hours after consumption respectively [Reygaert WC, 2017].

A pharmacokinetic study in rats has also revealed that after tea oral administration, about 14% of epigallocatechin, 31% of epicatechin, and <1% of epigallocatechin-3-gallate appeared in the blood. In humans, after administration of 3 g of decaffeinated green tea, the maximum plasma concentration for EGCG, EGC, and EC were 0.57, 1.60, and 0.6 μM respectively [Cai ZY, 2018].

The bioavailability of catechins can also be influenced by different processes including chemical degradation, microbial metabolism, intestinal and hepatic metabolism, membrane permeability, and transporter-mediators (*figure 5*) [Zhuo YC, 2018].

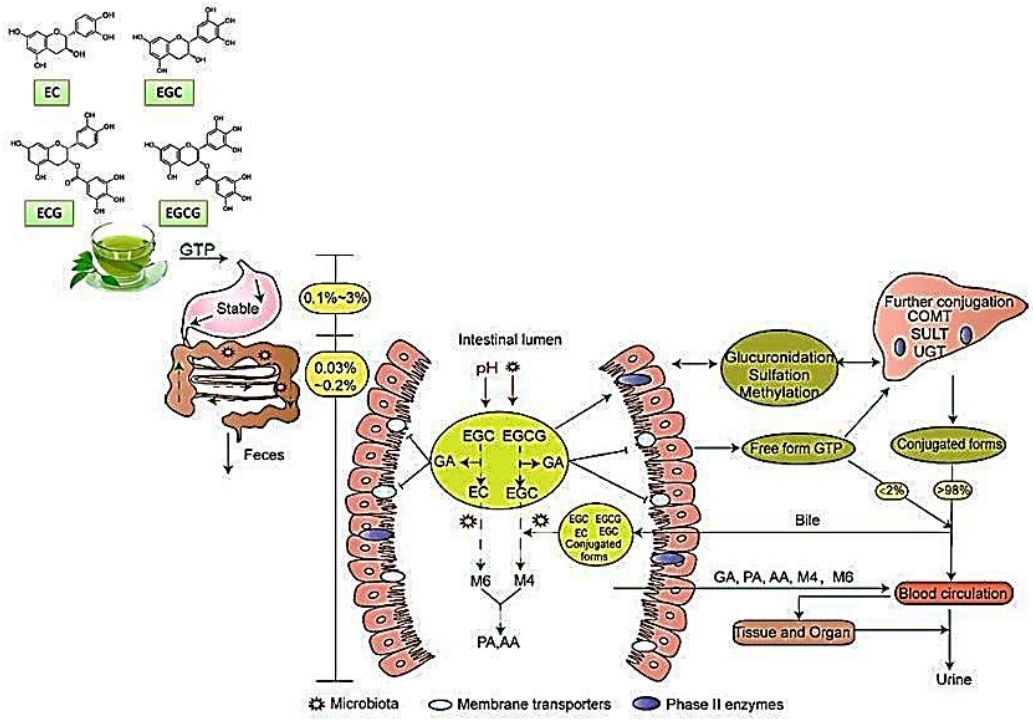

Figure 5. Bioaccessbility, bioavailbility, and metabolism of green tea polyphenols. GA: gallic acid; PA: phenolic acids; AA: aromatic acids; M6:5-(3′,4′-dihydroxyphenyl)-γ-valerolactone; M4:5-(3′,4′,5′-trihydroxyphenyl)-γ-valerolactone; membrane transporters (multidrug resistant proteins, adenosine triphosphate (ATP)-binding cassette transporters, P-glycoprotein); Phase II enzymes (COMT: catechol-O-methyltransferase; SULT: sulfotransferase; UGT: glucuronosyltransferases [modified from Xing L, 2019].

Upon absorption, a fraction of the ingested tea catechins were widely metabolized, both in small intestinal and the liver by phase II enzymes, such as UDP-glucuronosyltransferases (UGTs), sulphotransferases (SULTs), and catechol-O-methyltransferase (COMT) [Stalmach A, 2010].

Subsequently, catechin conjugates would reach the systemic circulation while most of them would go back to the gastrointestinal tract and eliminated via the bile. Glucuronidation and sulfation promote the solubility of catechins facilitating their elimination through urine. Consequently, the glucuronidated and sulphated conjugates of EGCG, EGC, and EC are commonly detected in human plasm and urine as well as their corresponding Omethyl-EGC-O-glucuronides and O-methyl-EC-O-sulfates [Chow HS, 2005; Xing L, 2019].

In the colon, the most abundant catechins may be further catabolized by the microflora into smaller molecular metabolites. EGCG was reported to be widely hydrolyzed leading to the production of EGC and gallic acid by the intestinal microbiota. The EGC may be further degraded into 5-(3′,4′,5′-trihydroxyphenyl)-γ-valerolactone in the large intestinal compartment. EC is further metabolized into 5-(3′,4′-dihydroxyphenyl)-γ-valerolactone and it is subjected to the same metabolic process as EGC. M4 and M6 are the major catechins catabolites resulting from the ring-fission activity of the intestinal microbiota [Actis-Goretta L, 2013; Xing L, 2019].

Therefore, green tea therapeutic potential is limited by its poor systemic absorption following oral administration, including low absorption, poor pharmacokinetics and bioavailability, scarce biodistribution, and low accumulation in related tissues of the body, or low targeting efficacy [Zhuo YC, 2018]. In this context, in the last years, some studies were performed in order to enhance the stability of GTCs. These studies have found that the bioavailability of catechins can be improved by nanostructure-based drug delivery systems, molecular modification, and co-administration with some other bioactive ingredients. In fact, encapsulation of tea catechins on protein-based, carbohydrate-based, and lipid-based nanoparticles improved stability, sustainable release and cell membrane permeation of catechins, resulting in increased bioavailability [Zhuo YC, 2018].

1.4.1 Antioxidant and anti-inflammatory activity

Green tea is a dietary source of antioxidant nutrients. It is rich in polyphenols but also contains carotenoids, tocopherols, ascorbic acid (vitamin C), minerals such as Cr, Mn, Se or Zn, that could increase the green tea antioxidant potential [Cambrera C, 2006].

Oxidative stress is known to be an important factor in aging and promotes the presence or complications of diseases such as atherosclerosis, diabetes mellitus, Alzheimer's disease or various types of cancer, as well as inflammatory processes [Pastoriza S, 2017]. It is considered a biochemical imbalance caused by an excessive production of reactive oxygen species (ROS), including oxygen ions, peroxide, and oxygen free radicals, or a decrease in oxidizing systems. ROS are naturally produced in cellular pathways of aerobic metabolism including oxidative phosphorylation, electron transport chains in mitochondria and microsomes, the activity of oxidoreductase enzymes, or even

immunological reactions such as active phagocytosis [Halliwell B, 2007]. However, high levels of ROS can cause damage to cellular and genetic structures [Droge W, 2002].

The antioxidant properties of green tea include the ability to limit the amount of free radicals by scavenging reactive oxygen and nitrogen species and chelating redoxactive transition metal ions [Gupta DA, 2014].

Green tea catechins may also function indirectly as antioxidant through: i) inhibition of the redox-sensitive transcription factors, pro-oxidant enzymes, such as inducible nitric oxide synthase (eNOS), lipoxygenases, cyclooxygenases and xanthine oxidase, and ii) induction of antioxidant enzymes, such as glutathione-S-transferases (GSTs), catalase (CAT) and superoxide dismutases (SOD) [Cabrera C, 2006].

Some human intervention studies have documented that a moderate consumption of green tea (1–6 cups per day) increases the total antioxidant capacity of the plasma by enhancing the organism protection against the oxidative damage caused by free radicals. Therefore, including the consumption of green tea in the usual diet has been recommended [Pastoriza S, 2017; Dai W, 2017].

Oxidative stress is closely tied to inflammation since ROS are capable of causing chronic inflammation through induction of inflammatory cytokines, chemokines, and pro-inflammatory transcription factors. Inflammation is a normal host defence mechanism that protects the host from infections and other insults but when inflammation is excessive, irreparable damage to host tissues and disease can occur. Indeed, chronic inflammation is considered a critical factor in many human diseases and conditions, including obesity, cardiovascular diseases, neurodegenerative diseases, diabetes, aging and cancer [Reygaert WC, 2017].

Several studies have shown that green tea affected the expression of inflammation-associated genes and proteins. Specifically GTCs increase the production of anti-inflammatory cytokine, e.g. interleukin (IL)-10, inhibit pro-inflammatory enzymes, such as cyclooxygenase 2, lipoxygenase, and inducible nitric oxide synthase (iNOS), and modulate signal transduction and transcription factors, including nuclear factor κB (NF-κB), activating protein 1 (AP-1), nuclear factor-erythroid 2-related factor 2 (Nfr2), mitogen-activated protein kinases (MAPK), and protein kinase C (PKC). They also are able to decrease the expression of different pro-inflammatory cytokines/chemokins, which include tumor necrosis factor (TNF)-α, IL-1β, IL-6, IL-8, and monocyte

chemoattractant protein 1 (MCP-1), in many cell types [Santangelo C, 2007; Ahmed S, 2008; Yun HJ, 2008; Serafini M, 2011].

Furthermore, the anti-inflammatory activities of catechins may be due to their suppression of neutrophil-endothelium interaction and subsequent transmigration by reducing the number of leukocyte-endothelial cell adhesion molecules (CAMs), such as intercellular adhesion molecule-1 (ICAM-1), vascular adhesion molecule-1 (VCAM-1), and E-selection, expressed on the endothelial cell surface [Donà M, 2003; Akhtar N, 2011].

1.4.2 Antimicrobial and antiviral properties

There is a large amount of research that has assessed the antimicrobial effects of GTCs on a wide variety of microorganisms, including many gram negative and gram positive bacteria (e.g., *Escherichiacoli*, *Salmonella* spp., *Staphylococcusaureus*, *Enterococcus* spp.), some fungi (e.g., *Candida albicans*), and a variety of viruses (e.g., HIV, herpessimplex, influenza) [Reygaert WC, 2014].

One of the major properties of GTCs is the ability to bind to the bacterial cell membranes damaging them, increasing their permeability, and leading to cell lysis. Bacterial cell membrane damage inhibits the ability of the bacteria to bind to each other to form biofilms, which are significant in pathogenesis [Reygaert WC, 2014]. Studies using human and mammalian cells lines have shown that, in presence of GTCs, various bacteria such as *Fusobacterium nucleatum*, *Staphylococcus epidermidis*, and *Helicobacter pylori,* have a significant decrease in their capacity to adhere to these cells [Lee KM, 2004; Lagha AB, 2017; Reygaert WC, 2018].

Green tea antimicrobial activity is mainly attributed to the inhibition of: i) the activity of the bacterial efflux pump responsible for secretion of toxins and efflux of substances, such as antimicrobial agents, ii) bacterial fatty acid biosynthesis by inhibiting enzymes involved in the biosynthetic pathway, iii) enzyme dihydrofolate reductase (DHFR) activity, and iv) other enzymes (e.g. protein tyrosine kinase, cysteine proteinases, DNA gyrase, ATP synthase) [Spina M, 2008; Wang Y, 2013; Reygaert WC, 2014].

Fatty acids in bacteria have important functions as a component of phospholipid cell membranes (and mycolic acid in cell walls of mycobacteria) and as an excellent energy source. Since this is an essential pathway for most bacteria, researchers are looking at targeting this pathway in antimicrobial drug development [Reygaert WC, 2014].

Studies on GTCs antimicrobial effects are providing promising results, especially because GTCs have also shown synergy with different known antimicrobial agents [Reygaert WC, 2018].

Moreover, some studies have shown a potential preventive effect of GTCs in viral infections by: inhibiting the virus binding to host cells as well as its entering (adenovirus, enterovirus, HBV, HCV, HIV, HSV, influenza, and rotavirus), inhibiting the viral RNA and DNA synthesis and viral gene transcription (enterovirus, EBV, HBV, HCV, and HIV), destroying and functionally altering various viral molecules (adenovirus, HSV, and influenza) [Reygaert WC, 2018].

1.4.3 Anticarcinogenic properties

The protective role of green tea against cancer has been supported by results from numerus studies in cell culture and animal model. Specifically, animal studies have shown that green tea consumption inhibits carcinogenesis of many types of cancer including lung, prostate, brest, skin, oral cavity, esophagus, stomach, liver, kidney, and other organs [Musial C, 2020]. The main chemopreventive effects of green tea depend on: i) its antioxidant action, ii) the specific induction of detoxifying enzimes, and iii) its molecular regulatory functions on cellular growth, development, and apoptosis [Cabrera C, 2006].

GTCs, especially EGCG, are involved in numerous signalling pathways and biological mechanisms related with cancer development and progression. Different studies have demonstrated that GTCs induce cell cycle arrest, regulating both G1/S and G2/M transition, and apoptosis in different cancer models without affecting normal cell [Subramani C, 2013]. Moreover, GTCs are able to induce both intrinsic (mitochondrial) and extrinsic (death receptor) apoptotic pathways. Nuclear condensation, caspase-3 activation, and poly(ADP)ribose polymerase cleavage are the main apoptotic features observed after treatment with GTCs [Musial C, 2020]. In addition, EGCG induced activation of pro-apoptotic proteins (BCL-2-associated X protein (BAX) and BCL-2 homologous antagonist killer (BAK)), depolarization of mitochondrial membranes, and cytochrome c release into cytosol [Kazi DM, 2002; Subramani C, 2013]. Other cancer related mechanisms attributed to EGCG are inhibition of: i) angiogenesis, ii) telomerase, iii) metalloproteinase activities, and iiii) NF-kB that plays a critical role in the regulation

of a variety of genes important in cellular responses, including inflammation, proliferation, and cancer cell death [Lambert JD, 2010; Reygaert WC, 2017].

In vitro and *in vivo* studies have shown that GTCs are able to regulate even more molecular signalling pathways implicated in cancer development and progression such as the epidermal growth factor receptor (EGFR)-mediated signal transduction pathway and insulin-like growth factor-I (IGF I)-mediated signal transduction pathway [Musial C, 2020]. Furthermore, available literature data indicate that polyphenols derived from green tea can prevent cancer by modulating epigenetic aberrations taking place in DNA methylation, histons, and micro-RNAs [Fang MZ, 2003; Bag A, 2018].

The anticancer potential of GTCs has also been studied in cancer stem cells which are characterized by the ability to proliferate and maintain a constant, unchanging number of cells. *In vivo* and *in vitro* studies report that cancer stem cells are responsible for cancer renewal as well as metastasis [Musial C, 2020].

Despite the great potential as an anti-cancer agent, the use of EGCG in clinical settings is limiting due to its short half-life, low stability and low bioavailability. In recent years, particular attention has been given to the nano-chemoprevention, a strategy based on the use of nanotechnology to improve the pharmacokinetic and pharmacodynamic of chemopreventive agents [Granja A, 2016]. Several studies have already applied this strategy encapsulating EGCG into different types of nanoparticles, including gold, polymeric, metallic, carbohydrate-based and liposomes, for cancer treatment. The results revealed that EGCG nanoparticles are capable to prolong circulation time in blood, increase cell internalization in tumor sites, and inhibit tumor growth predominantly in *in vitro* and *in vivo* breast and prostate cancer models [Granja A, 2016].

1.4.4 Cardiovascular Disease health benefits

Cardiovascular diseases (CVDs) represent a group of heart and blood vessels disorders, mainly including coronary heart disease (CHD), stroke, heart failure, hypertensive heart disease, and rheumatic heart disease [Eng QY, 2018]. CVDs are the leading causes of morbidity and mortality in industrialized countries. According to World Health Organization report, CVDs were accounted for 29% of all global deaths in 2004 and about 23.6 million people will die from CVDs by 2030 [Islam MA, 2012].

Epidemiological and clinical studies in humans suggest that a regular consumption of green tea may be associated with a lower cardiovascular risk [Pastoriza S, 2017]. Several

studies in Japan population reported a significant decrease in cardiovascular disease mortality in individual who consumed ≥5 cups of green tea per day compared with those drinking one cup per day or none [Nakachi K, 2000; Suzuki E, 2009]. Another study on Japanese women and man with visceral fat-type obesity consuming green tea extracts for 12 weeks showed a reduction in body fat (10%), blood pressure (6.5%), and low-density lipoprotein (LDL) levels (2.6%), suggesting reduced risk for CVDs [Nagao T, 2007].

The cardioprotective effect of green tea was also demonstrated in numerous *in vitro* and animal studies. GTCs are able to prevent atherosclerosis, hypertension, endothelial dysfunction, ischemic heart diseases, cardiomyopathy, cardiac hypertrophy, and congestive heart failure by decreasing oxidative stress, preventing inflammatory events, reducing platelet aggregation, and halting the proliferation of vascular smooth muscle cells [Bhardwaj P, 2013].

Antioxidant Effect

Oxidative stress plays a central role in the progression of different CVDs, including atherosclerosis, hypertension, endothelial dysfunction, ischemic heart diseases, cardiomyopathy, cardiac hypertrophy, and congestive heart failure. An increase of ROS formation and/or decreased of antioxidant enzymes cause oxidative stress triggering to a rapid depolarization of mitochondrial inner membrane potential and subsequent impairment of oxidative phosphorylation in cardiac and vascular myocytes. Damaged mitochondria, in turn, produce further ROS, mainly in the form of the superoxide anion (O_2^-) and hydrogen peroxide (H_2O_2) [Bhardwaj P, 2013].

Green tea caused an increase in the activity of enzymes implicated in cellular protection against reactive oxygen species like superoxide dismutase in serum and catalase in the aorta. Catechins also inhibit the redox-sensitive transcription factors, NF-κB and AP-1, responsible for oxidative stress. This is combined with a direct action on oxygen species by modulating pro-oxidant enzymes, such as inducible nitric oxide synthase, lipoxygenase, cyclooxygenase, and xanthine oxidase [Khan N, 2013].

The high concentration of ROS impairs cardiovascular function by inducing vascular smooth muscle cells (VSMC) proliferation, vascular endothelial dysfunction (VED), and cardiac apoptosis and/or necrosis [Bhardwaj P, 2013].

Effect on Vascular Homeostasis

Vascular endothelial dysfunction is a systemic pathological state of the endothelium, involved in the pathogenesis of various cardiovascular disorders such as hypertension, atherosclerosis, coronary artery diseases, diabetes mellitus, and nephropathy [Bhardwaj P, 2013].

Endothelial cells play a central role in maintaining vascular homeostasis by balancing vasoconstrictive substances, such as endothelin-1 (ET-1), prostaglandins, angiotensin II (Ang-II) and vasodilating substances, such as nitric oxide (NO), prostacyclin, and various endothelium derived hyperpolarizing factors (EDHFs) [Bhardwaj P, 2013]. Endothelium-derived NO, synthesized from L-arginine by endothelial isoform of NO synthase, is not only a vasodilator, but also inhibits the expression of leukocyte adhesion molecules at the endothelial surface. For this reason, NO blocks the adherence of leukocytes to endothelial cells, thereby preventing platelet adhesion and aggregation and inhibiting the proliferation of VSMCs. Thus, endothelial dysfunction and the subsequent impairment of NO production is widely acknowledged as a critical step in the initiation of atherogenesis and vascular pathogenesis [Islam MA, 2012].

Experimental and clinical studies suggest that GTCs can significantly improve endothelial function and reduce blood pressure by: i) increasing NO production through the activation of eNOS and ii) reducing the endogenous asymmetric dimethylarginine (ADMA) level, which competes with L-arginine and reduces NO production in the vascular wall [Tang WJ, 2006; Yamagata K, 2019].

Anti-Platelet Activity and Anti-Thrombotic Effect

In the presence of vascular endothelial injury, platelets usually respond rapidly and aggregate to form a prothrombotic surface that promotes clot formation and subsequently vascular occlusion. Platelet activation and aggregation are hallmarks of CVDs, such as myocardial infarction and stroke [Islam MA, 2012; Bhardwaj P, 2013].

Both, *in vitro* and *in vivo* studies have shown that GTCs are involved in the inhibition of platelet aggregation affecting several cellular targets, including: i) the arachadonic acid pathway, ii) calcium cytoplasmic increase, iii) thromboxane A2 (TXA2) production, and iv) cyclooxygenase-1 (COX-1) [Son DJ, 2004; Jin YR, 2008; Lee DH, 2013].

In addition, EGCG hampers platelet activation by adenosine diphosphate (ADP) stimulation and suppress the p38 mitogen-activated protein kinase phosphorylation of heat shock protein 27 (HSP27), which, in turn, would inhibit the release of pro-thrombotic contents from platelets [Iida Y, 2014].

Anti-inflammatory effect

Vascular inflammation is considered as a key process in the pathogenesis of atherosclerosis that is initiated with the adhesion of monocytes to the vascular endothelial cells and their subsequent transmigration into the sub-endothelial intima. A pivotal role in the binding of leukocytes to the sites of inflammation is played by ICAM-1 and VCAM-1, which are regulated by NF-kB. Once adhered to the endothelium, the leukocytes penetrate into the intima at the sites of lesion formation attracted by chemotactic molecules, such as MCP-1, IL-8, and E-selectin. Further, macrophage colony-stimulating factor (MC-SF) contributes to the transmigration of monocytes into the intima [Bhardwaj P, 2013].

GTCs prevent inflammation-mediated atherosclerosis by suppressing leukocyte adhesion to the endothelium and its subsequent transmigration. Studies have shown that GTCs reduce the expression of pro-inflammatory cytokines, chemokines, and adhesion molecules that are regulated by NF-κB and suppress myocardial inflammation. Moreover, *in vitro* studies have shown that EGCG could suppress the expression of VCAM-1 reducing the leukocyte adhesion to endothelial cells, and decrease MCP-1 expression responsible for inflammation [Ludwig A, 2004; Hong MH, 2007; Reygaert WC, 2017]. EGCG was also shown to suppress the pro-inflammatory actions of TNF-α through over expression of heme oxygenase-1 in vascular endothelial cells via p38 MAPK and Nrf-2 signalling pathways [Pullikotil P, 2011].

Anti-proliferative effect

In addition to inflammation, a key process of atherosclerosis involves the proliferation of vascular smooth muscle cells to the sub-endothelial space. In early atherosclerosis, VSMCs may contribute to the development of the atheroma through the production of pro-inflammatory mediators, such as monocyte MCP-1, VCAM, and matrix metalloproteinases [Bhardwaj P, 2013].

GTCs have been shown to prevent matrix protein degradation and cell migration by inhibiting expression or activity of MMP-2 and MMP-9, in a dose-dependent manner [El Bedoui J, 2005; Kim CH, 2005].

Catechins can also modulate the factors responsible for VSMCs proliferation. Indeed, EGCG treatment has been shown to arrest VSMCs in the G1 phase of the cell cycle by down-regulating important cell cycle regulators, such as cyclins/cyclin-dependent kinases [Bhardwaj P, 2013]. Furthermore, EGCG can inhibit VSMC proliferation induced by high glucose, and angiotensin-II [Won SM, 2006; Yang J, 2011].

Effect on Lipid Metabolism

Hyperlipidemia, resulting from the abnormalities of lipid metabolism, is one of the major risk factors for the development of CVDs. The elevated levels of plasma lipids such as fatty acids, cholesterol, phospholipids and triglycerides can lead to the development of atherosclerotic plaques [Jain KS, 2007].

GTCs affect lipid metabolism by various mechanisms and prevent the appearance of atherosclerotic plaque in various models of hyperlipidemia. Studies demonstrated that GTCs modulate cholesterol metabolism mainly by targeting its biosynthesis and intestinal absorption [Bursill CA, 2007; Koo SI, 2007].

Tea catechins enhance intestinal lipid absorption through direct interference with lipid emulsification, hydrolysis, and micellar solubilisation [Islam MA, 2012]. The micellar solubilisation of hydrolysed lipids, a critical step for the uptake and absorption of lipids by enterocytes, facilitates the transfer of lipids through the unstirred water layer to the enterocyte for the uptake [Koo SI, 2007].

Furthermore, catechins can up-regulate hepatic low-density lipoprotein receptor expression thereby modulating biosynthesis, excretion, and intracellular processing of lipids [Koo SI, 2007]. Humans studies have reported that consumption of GTCs lowers total cholesterol and LDL levels, and improved protective HDL cholesterol [Kim A, 2011]. In addition, extensive *in vitro* and *in vivo* studies reported that GTCs protect LDL from oxidation through incorporating themselves into LDL particles [Erba D, 2005; Suzuki-Sugihara N, 2016]. Oxidation of LDL played a central role in the pathogenesis of arteriosclerosis. Oxidized LDL induces modifications in lipoproteins, stimulates inflammatory reactions, causes monocytes and monocyte-derived macrophages to

uptake oxidized LDL, and ultimately leads to the formation of lipid-loaden foam cells and atherosclerotic plaques. These plaques protrude from the inner surface of the arteries narrowing the lumen, reducing the blood flow, and leading to coronary heart disease [Jain KS, 2007].

The modulation of all these molecular events by GTCs improves oxidative status, lipid profile, and vascular homeostasis while inhibits vascular inflammation, thrombosis, and VSMC growth and migration, thereby preventing CVDs (*figure 6*).

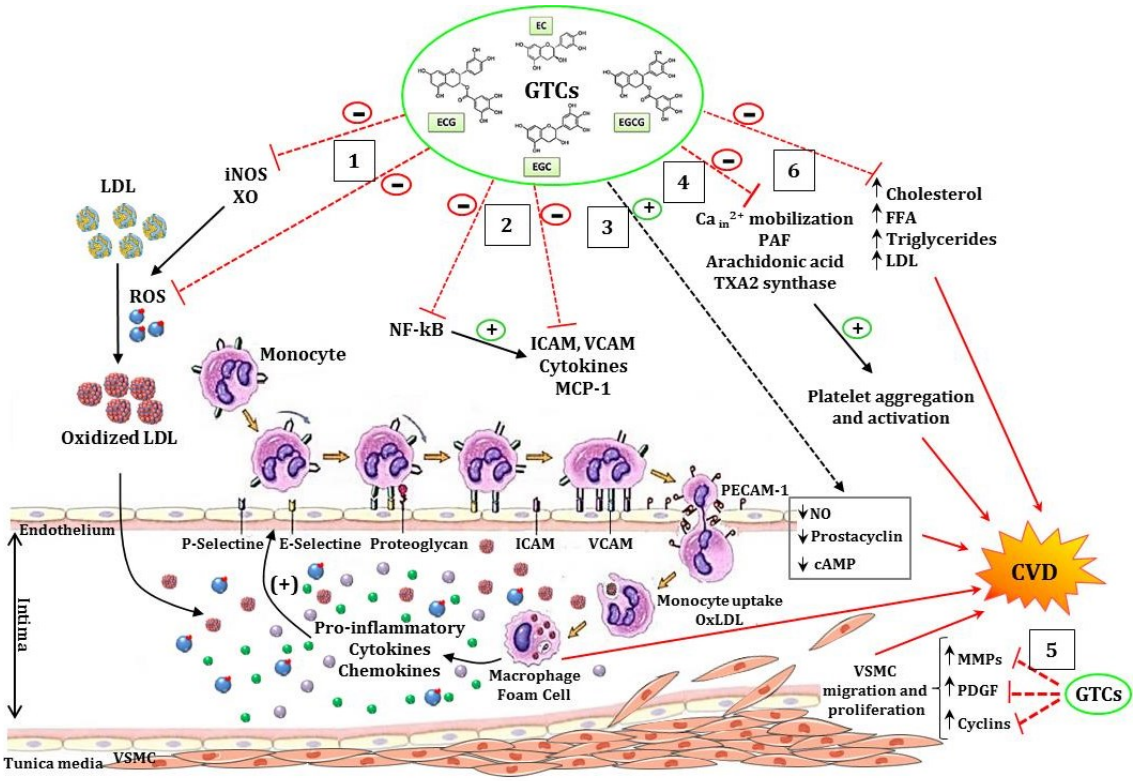

Figure 6. Schematic representation of the main mechanisms underlying the vascular protective effects of green tea catechins: (1) scavenging free radicals and inhibiting pro-oxidant enzymes, which in turn inhibit ROS induced oxidative stress and LDL oxidation; (2) preventing adhesion of monocytes to the endothelium and the consequent transendothelial migration by the inhibition of NF-kB, cytokine, and adhesion molecules; (3) stimulating NO endothelial production prostacyclin, and cAMP; (4) decreasing platelet aggregation and activation by reducing intracellular calcium mobilization, PAF and arachidonic acid release, and thromboxane A2 synthase; (5) inhibiting cyclins, PDGF, and MMPs; (6) increasing intestinal lipid excretion, by the inhibition of cholesterol, fatty acids (FFA), and triglycerides absorption and synthesis.

Protecting Cardiomyocyte Function

Mechanistic studies have demonstrated that green tea polyphenols may influence many aspects of cardiovascular function by interacting with a list of intracellular target, such

as several ion channels and ion exchangers (Na^+/K^+- ATPase, Na^+/H^+, and Na^+/Ca^{2+}), intracellular Ca^{2+} storage, and sarcomeric troponin protein [Kargacin ME, 2011; Lorenz M, 2008; Pan B, 2017].

There is also evidence that the epigallocatechin-3-gallate may modulate myocardial contractility. A study reported that EGCG acute administration in cardiomyocytes isolated from a transgenic mice model of hypertrophic cardiomyopathy, ameliorated sarcomere shortening and lowered relaxation time by decreasing the thin myofilament Ca^{2+} sensitivity [Friedrich FW, 2016].

Recent data suggest that green tea exerts its beneficial effects by improving myocardial reperfusion-induced injury, attenuating myocardial remodelling after experimental myocardial infarction, and ameliorating systolic and diastolic dysfunction. Moreover, green tea has positive inotropic and anti-hypertrophic properties [Potenza MA, 2007; Lustosa BB, 2016; Garcia ML, 2017].

Nevertheless, to provide a better understanding of GTCs mechanisms of action, their molecular targets and mediated signalling pathways, have to be further clarified [Cao SY, 2019].

1.5 Diabetic cardiomyopathy and its pathophysiological mechanisms

Cardiovascular diseases are the leading cause of morbidity and mortality in patients with both type 1 and type 2 diabetes. In particular, about 55% of the diabetic patients present diabetic cardiomyopathy (DCM), independent of the coexistence of other cardiac pathologies [Al Hroob AM, 2019].

DCM is a specific heart condition which originates in cardiac muscle of diabetic subjects and affects myocardial structure, function, and metabolism in the absence of coronary artery disease (CAD), ischemic heart or hypertension. DCM is characterized by diastolic dysfunction followed by abnormalities in systolic function, cardiac remodelling, and hypertrophy as well as altered cardiac energy metabolism [Athithan L, 2019].

Molecular mechanisms underlying these pathological changes in the diabetic heart are complex, multifactorial, and include, but not limited to, oxidative stress, inflammation, cell death, endothelial dysfunction, fibrosis, cardiac lipotoxicity, and energetic impairment (*figure 7*) [Al Hroob AM, 2019].

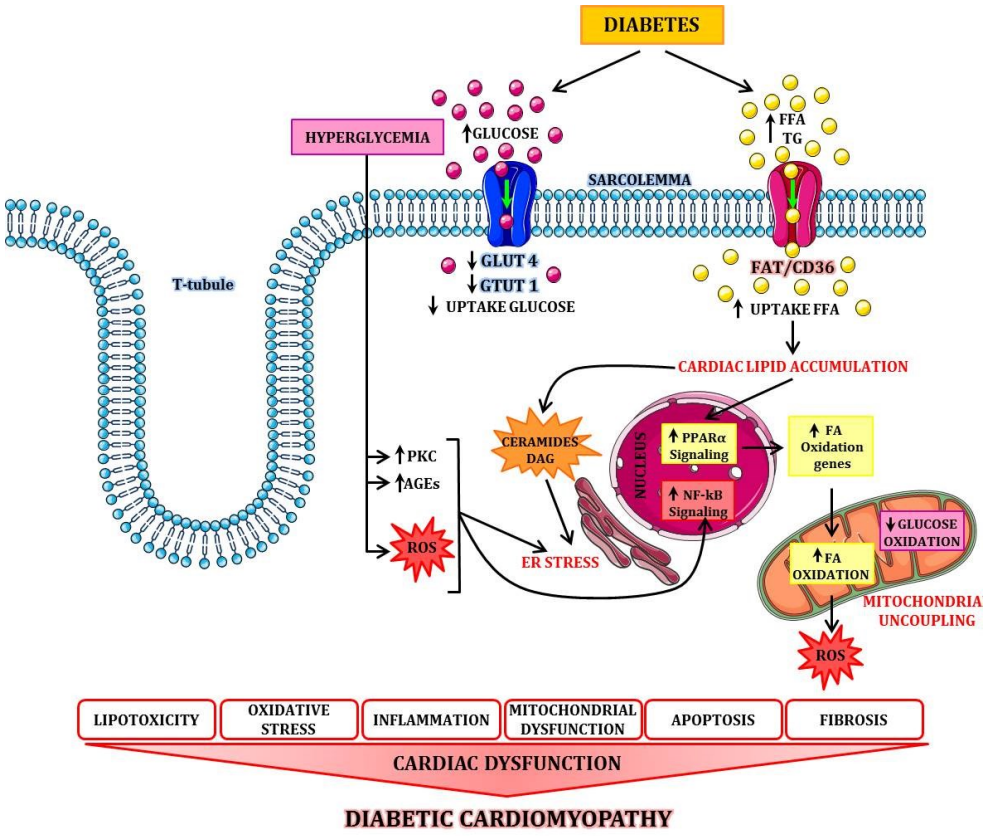

Figure 7. Major pathophysiological mechanisms of DCM.

Hyperglycemia and dyslipidemia are the central players in activating several adaptive and maladaptive responses in myocardial tissue among which cellular oxidative stress and moderate tissue inflammation constitute critical early pathogenic components [Bugger H, 2014].

Human and animal studies have reported that the long-standing hyperglycemia triggers the generation of ROS from mitochondria, the reduction in the activity of antioxidant enzyme glutathione reductase (GSR), and the formation of advanced glycation end-products (AGEs) [Yamagishi SI, 2015]. Accumulation of AGEs in the diabetic heart can cause irreversible glycosylation of structural proteins, including Ca^{2+} channels. At the same time, AGEs can increase myocardial collagen cross-linking leading to myocardial fibrosis and subsequently impaired cardiac relaxation and diastolic and systolic dysfunction [Bugger H, 2014; Yamagishi SI, 2015].

Other than a direct damage, AGEs also contribute to ROS generation and inflammation via activation of AGE receptors (RAGE), which can activate NF-kB causing increased release of pro-inflammatory cytokines [Bugger H, 2014].

Uncontrolled oxidative stress caused by ROS increase can provoke protein and lipid oxidation that also play an important role in the development of DCM [Liu Q, 2014]. Specifically, ROS-mediated oxidative modification of protein in diabetic heart can affect membrane structure, protein folding, transcription factors, excitation-contraction coupling, and contractility, causing myocardial dysfunction. Moreover, lipid peroxidation can disrupt the membrane lipid bilayer arrangement, inactivate membrane-bound receptors and enzymes and increase tissue permeability inducing cardiomyocytes damage [Giacco F, 2010; Varga ZV, 2015; Al Hroob, 2019].

Furthermore a marked correlation between hyperglycemia state and oxidative DNA damage was reported. ROS are able to induce multiple DNA modification, such as single and double strand breaks, oxidized DNA bases, chemical and structural modification to purine and pyrimidine [Al Hroob AM, 2019].

In particular, numerous studies reported that poly (ADP-ribose) polymerase-1 (PARP-1) is overexpressed in response to oxidative stress-induced DNA damage, resulting in structural and functional alterations in the diabetic heart [Al Hroob AM, 2019]. PARP-1 over-activation can facilitate the translocation of NF-kB and the production of a variety of pro-inflammatory mediators leading to increased inflammation and associated oxidative stress [Chiu J, 2008; Bugger H 2014]. Studies performed in rodent model have shown that the high-glucose triggers the synthesis and release of pro-inflammatory chemokines in cardiomyocytes and cardiac fibroblasts, suggesting that both cell compartments contribute to divert myocardial environment since the early stages of the disease [Savi M, 2016].

Apart from hyperglycemia, chronic dyslipidemia has emerged as a major factor in the pathogenesis of cardiac complication and atherosclerosis in diabetic population [Nelson RH, 2013]. In diabetes, a decrease in insulin sensitivity leads to an inability to suppress lipase within adipose tissue and very low-density lipoprotein within the liver. This results in high levels of circulating fatty acid (FA) and triglyceride (TG) and as a consequence peroxisome proliferator activated receptor-α (PPARα) activation, which determines FA oxidative capacity by increasing FA oxidation gene expression [Athithan L, 2019]. Concomitantly, glucose uptake, glycolysis and glucose oxidation are reduced in the diabetic heart, most likely mediated by decreased glucose-transporter-4 (GLUT4) expression and activity [Finck BN, 2002; Athithan L, 2019].

Indeed, diabetic dyslipidemia may induce ectopic lipid accumulation in cardiac myocytes, resulting in the increased ROS production, oxidative degradation of lipids and membrane destabilization that can cause cardiomyocyte dysfunction through apoptosis [Chong CR, 2017].

High levels of FA oxidation results in increased intracellular long chain fatty acyl-CoA concentration and consequently lipotoxic intermediates production, such as ceramide and diacyl-glycerol (DAG) [Wende AR, 2012]. In addition, several studies have shown that the elevated FA oxidation in diabetic hearts improves myocardial oxygen consumption, which is not accompanied by an equivalent increase in ATP production, leading to mitochondrial uncoupling. This uncoupling is mediated by increased proton flux through mitochondrial uncoupling proteins (UCP), which are activated by reactive oxygen radicals. FA-induced mitochondrial uncoupling results in energy depletion and decrease in cardiac efficiency [Mazumder PK, 2004; Boudina S, 2007; H. Bugger, 2014].

Another important lipotoxicity consequence is the remodelling of the mitochondrial membrane phospholipid composition, including a decrease in cardiolipin content and an increase in the saturated lipid content of the endoplasmic reticulum (ER) resulting in ER stress [Ostrander DB, 2001; Borradaile NM, 2006].

Accordingly, extensive evidence suggests that mitochondrial dysfunction and altered myocardial energy metabolism have an important contribution to the development and progression of DCM [Duncan JG, 2011]. Mechanisms underlying mitochondrial dysfunction and impairment in mitochondrial morphology include oxidative damage, mitochondrial uncoupling, transcriptional and translational alterations of oxidative phosphorylation (OXPHOS) subunit expression, impaired mitochondrial calcium handling, changes in cardiac insulin signalling, and altered mitochondrial dynamics and biogenesis [H. Bugger, 2010; Konig A, 2012; Al Hroob, 2019].

Hyperglycemia, dislipidemia, oxidative stress, increased circulating inflammatory cytokines, up-regulation of the renin–angiotensin–aldosterone system (RAAS), and mitochondrial dysfunction can cause caspase activation, altered expression of anti- and pro-apoptotic protein and an increase in the rate of apoptosis in cardiomyocytes [Al Hroob AM, 2019]. Specifically, loss of cardiomyocytes due to apoptosis stimulates resident cardiomyocyte hypertrophy and fibroblast proliferation, causing cardiac concentric remodelling and then heart failure [Liu Q, 2014; Levelt E, 2016].

The major structural alterations observed in diabetic heart are an increase in left ventricular mass and wall thickness, perivascular and intermyofibrillar fibrosis, and cardiac steatosis [Bugger H, 2014; Al Hroob AM, 2019]. Moreover, high circulating glucose concentration may cause coronary microvascular dysfunction by downregulating nitric oxide. This, in turn, increases vasoconstriction, vascular tone, permeability, thinning of vascular endothelium and weakening of intercellular junctions [Sucato V, 2015].

Altogether, these structural alterations lead to cardiac dysfunction characterized by an impaired diastolic function followed by altered systolic function at later stages of the disease, resulting in symptomatic heart failure and left ventricular dilation [Shang Y, 2017].

Identify metabolic and structural changes in the heart as soon as possible is essential in order to prevent the progressive impairment of cardiac structure and function that , in time, leading to irreversible heart failure [Grigorescu ED, 2019].

Indeed, despite prominent advances in diabetes prevention, treatment, glucose monitoring, and novel glycemic control biomarkers, DCM detrimental cardiovascular complications, still remain severe in diabetic patients. Therefore, more studies are needed to: i) understand the potential mechanisms, some of these still under-investigated, involved in the pathophysiology of DCM and ii) develop novel cardioprotective strategies toward prevention and amelioration of diabetes-related cardiovascular complications [Al Hroob AM, 2019].

2. AIM of THE STUDY

Growing evidence has established a close relationship between the consumption of green tea polyphenols and the risk reduction of several pathological conditions including CVDs. GTCs exert vascular and myocardial protective effects through multiple mechanisms, including anti-oxidative, anti-hypertensive, anti-inflammatory, anti-proliferative, anti-thrombogenic, and lipid lowering effects [Cao SY, 2019]. Previous experimental studies have documented that tea extracts, especially EGCG, are able to attenuate reperfusion-induced myocardial damage, cardiac hypertrophic response to pressure-overload, sympathetic hyperactivity in hypertension, and ventricular dysfunction in several cardiomyopathies [Potenza MA, 2007; Friedrich FW, 2016; Lustosa BB, 2016; Pan B, 2017; Garcia ML, 2017].

However, most studies refer to the effects of acute exposure to GTCs and have been performed on cell lines, perfused rat hearts, isolated cardiomyocytes, subcellular cardiomyocyte organelles and *in silico* models [Hotta Y, 2006; Lorenz M, 2008; Kargacin ME, 2011; Fuchs F, 2013; Boukhabza M, 2016]. Conversely, studies showing potential positive effects on normal heart of *in vivo* long term administration of GTCs, are still lacking. Moreover, even if the daily consumption of green tea or its extract is considered safe, there is still discordance about the beneficial effects [Xing L, 2019].

The present work was divided into two different parts:

1. the **first part** was aimed at comparing the effects of standardized green tea extracts (GTE) and their major component EGCG, given at the equivalent amount that would be in the entirety of GTE, on cardiac function [Bocchi L, 2018; Vilella R, 2020]. We addressed this issue following an experimental approach which involved *in vivo* and *ex vivo* measurement of contractile properties in normal rats, focusing on the underlying molecular mechanism and mitochondrial bioenergetics.
2. the **second part** was focused on investigating the ability of early GTE administration to prevent the development of cardiomyocyte contractile dysfunction induced by a short period of hyperglycemia. It is well known, in fact, as since the early stage of diabetes, hyperglycemia and the associated metabolic dysregulation induced oxidative stress and upregulation of inflammatory cytokines that impair cardiac function and promote structural damage, progressively leading to the diabetic cardiomyopathy phenotype [Stilli D, 2007;

Savi M, 2016]. Emerging evidence suggest that polyphenols may constitute a new preventive strategy to counteract the occurrence and/or the progression of cardiomyopathies in which oxidative stress, myocardial tissue inflammation, mitochondrial dysfunction, and changes of expression and/or activity of contractile proteins constitute early pathogenic factors [Santos CN, 2018; Viola HM, 2019]. To specifically address this issue, cardiomyocyte contractile properties and intracellular calcium dynamics were measured in a rat model of early diabetes, after *in vivo* administration of GTE.

3. MATERIALS and METHODS

3.1 Animals and housing

The study population consisted of 60 male Wistar rats (*Rattus Norvegicus*) aged 12-18 weeks, individually housed in a temperature-controlled room at 22–24 °C in which the light was kept on between 7 a.m. and 7 p.m.. The bedding of the cages consisted of wood shavings, and food was freely available (Mucedola s.r.l., Milan, Italy). The investigation was approved by the Veterinary Animal Care and Use Committee of the University of Parma-Italy (Prot. N°614/2016-PR) and conforms to the National Ethical Guidelines of the Italian Ministry of Health and the Guide for the Care and Use of Laboratory Animals (National Institute of Health, Bethesda, MD, USA, revised 1996). All experiments were carried out in accordance with the approved guidelines. Every effort was made to minimize animal suffering.

3.2 Experimental protocol part 1 (EXP.1)

The first part of the present study was scheduled in two sets of experiments: EXP.1a (*figure 8*) and EXP. 1b (*figure 9*).

3.2.1 EXP.1a

Twenty rats, aged 12-14 weeks, weighing 414 ± 9.6 g (mean ± standard error of the mean) were randomly divided into two experimental groups: **CTRL** group (*n=10*), receiving 40 mL/day of tap water for 28 days and used as controls and **GTE** group (*n=10*), receiving 90 mg/day of standardized GTE in 40 mL of tap water for 28 days. The optimal administered solution volume was previously determined and represents the lowest value of the range of daily water consumption in male rats, matched for age and body weight. The solution was freshly prepared in tap water and orally administered every day to the experimental animals in dark bottles to prevent its oxidation. The GTE concentration choose for this study is well tolerated by rats and does not cause side effects. Moreover, this protocol has been used in past by other investigators [Adhami VM, 2009; Kim SJ, 2014].

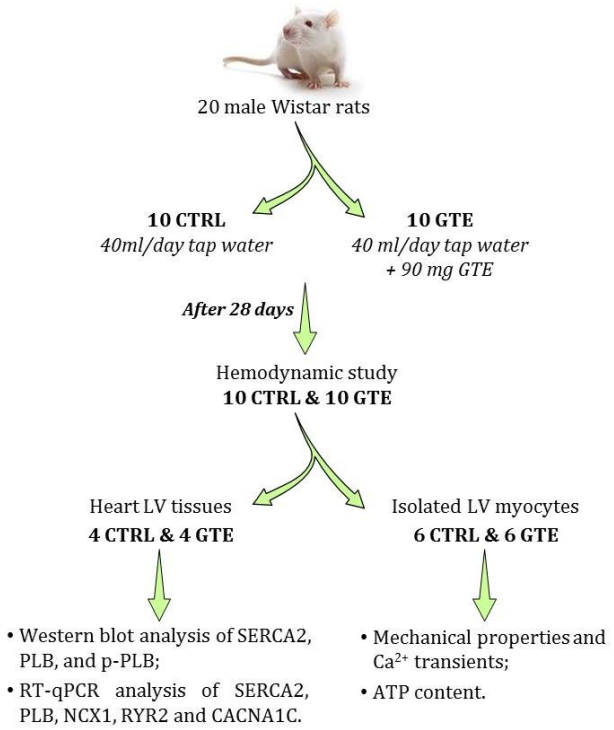

Figure 8. Schematic diagram showing EXP.1a protocol. SERCA2: Sarco-Endoplasmic Reticulum Calcium ATPase 2; PLB: Phospholamban; p-PLB: phospho-Phospholamban; NCX1: Na^{+}-Ca^{2+} exchanger; RYR2: Ryanodine receptor 2; CACNA1C: Calcium voltage-gated channel subunit alpha1 C.

The rat body weights were measured every week until sacrifice. After 4 weeks of treatment, hemodynamic measurements were performed in all CTRL and GTE rats anesthetized with ketamine chloride (Imalgene, Merial, Milan, Italy; 40 mg/kg i.p.) plus medetomidine hydrochloride (Domitor, Pfizer Italia S.r.l., Latina, Italy; 0.15 mg/kg i.p.). Immediately after hemodynamic measurements, in subgroups of each experimental group (6 CTRL and 6 GTE), the heart was excised and cardiac cells were enzymatically isolated to measure cardiomyocyte mechanical properties and calcium transients.

A fraction of isolated left ventricle myocytes was washed three times with low-calcium solution (0.1 mM) and centrifuged (500 rpm for 5 min). After removing the supernatant, the pellet was stored at -80°C for the subsequent evaluation of ATP content. From the remaining 8 rats (4 CTRL and 4 GTE), the heart was rapidly excised and perfused with a 0.9% NaCl solution at 37°C to drain the residual blood. Then, the tissues (left ventricles) were snap frozen in liquid nitrogen and stored at -80°C for molecular analyses.

3.2.2 EXP.1b

To investigate the mechanisms underlying GTE action in comparison to its major catechin, EGCG, given at the equivalent amount that would be in the entirety of GTE, twenty six additional rats, aged 16–18 weeks, weighing 425.5±6.3 g, were studied.

The animals were divided into the following groups: (1) **CTRL** group (*n=8*), receiving 40 mL/day of tap water, (2) **GTE** group (*n=9*), receiving 40ml/day of tap water solution of GTE as previously described, and (3) **EGCG** group (*n=9*), receiving 63 mg/day of EGCG (Epigallocatechin-3-gallate Sigma-Aldrich, Milan, Italy) in 40 ml of tap water, for 28 days. Body weight was measured once a week until sacrifice, after 4 weeks of treatment. At the end of the experimental protocol:

A. the hearts of 15 animals (5 GTE, 5 EGCG and 5 CTRL) were excised and cardiac cells were enzymatically isolated and used for: i) measuring cell mechanical properties and calcium transients, ii) evaluating mitochondrial activity, and iii) subsequent biochemical analysis after storing the cells at -80°C.

B. the hearts of 8 rats (3 GTE, 3 EGCG and 2 CTRL) were excised after perfusion with 0.9% NaCl solution at 37°C and the left ventricles (LV) were snap frozen in liquid nitrogen and stored at -80°C for subsequent molecular analyses.

C. the hearts of the remaining animals were arrested in diastole by perfusion with $CdCl_2$ (100 mM) and used for transmission electron microscopy analysis (TEM).

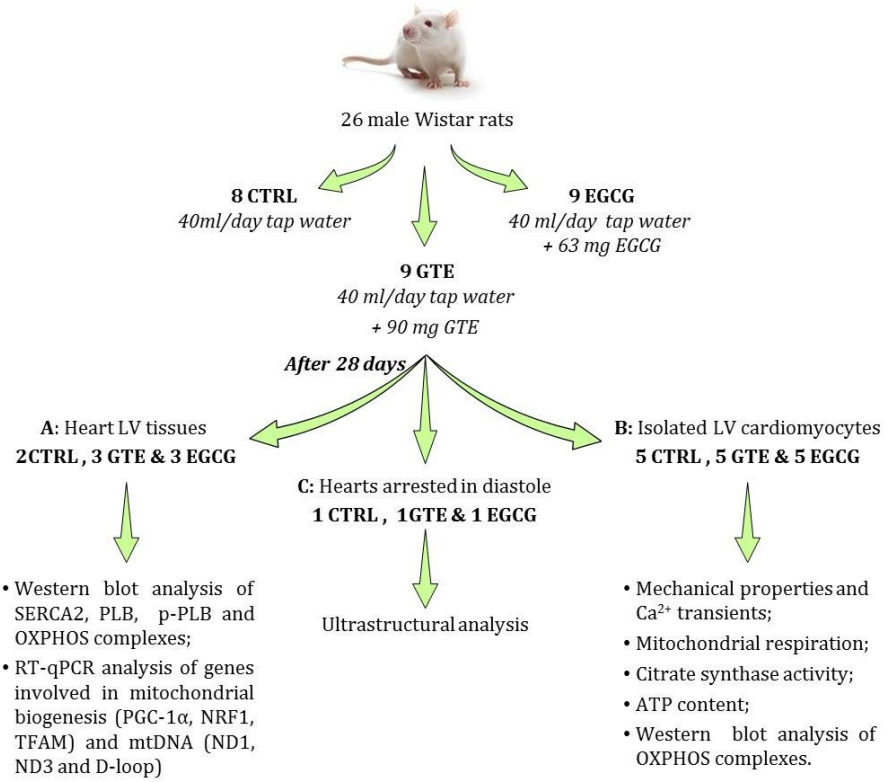

Figure 9. Schematic diagram illustrating the EXP.1b protocol. OXPHOS: oxidative phosphorylation; PGC-1α: peroxisome proliferator-activated receptor gamma coactivator 1-alpha; NRF1: nuclear respiratory factor 1; TFAM: mitochondrial transcription factor A; mtDNA: mitochondrial DNA; ND1: NADH-ubiquinone oxidoreductase subunit 1; ND3: NADH-ubiquinone oxidoreductase subunit 3; D-loop: displacement loop region of mitochondrial DNA.

3.3 Experimental protocol part 2 (EXP.2)

The study population consisted of 14 male Wistar rats, aged 14-16 weeks, weighing 376.3 ± 4.2 g. Five rats were used as the control group (**CTRL**) while in the remaining nine animals type-1 diabetes was induced (group D) by a single intra-peritoneal (i.p.) injection of streptozotocin (STZ, 60 mg/kg, Sigma-Aldrich, Milan, Italy). Glucose blood levels and body weights were measured in 4-h-fasting animals two days after the STZ injection and weekly until sacrifice, 3 weeks after the induction of hyperglycaemia. After the documented increase in blood glucose levels (2 days after STZ injection; blood glucose cut-off: 250 mg/dl), D animals were divided in two groups: **D3** group (n =4) and **D3_GTE** group (n=5). Only D3-GTE group was subjected to chronic GTE oral administration (90mg/day of GTE dissolved in 50ml of tap water) for 21 days. After 3 weeks of hyperglycaemia, all the animals were anesthetized, the heart was rapidly removed, and ventricular cardiomyocytes were enzymatically isolated for the *ex vivo* measurement of cell mechanical properties and calcium transients.

3.4 Hemodynamic study

Invasive hemodynamic data were recorded in 20 healthy rats (10 CTRL and 10 GTE). After anaesthesia a microtip pressure transducer catheter (Millar SPC-320, Millar Instruments, Houston, TX, USA) connected to a recording system (Power Laboratory ML 845/4 channels, 2Biological Instruments, Besozzo, Italy), was inserted into the right carotid artery to record systolic and diastolic blood pressures. The catheter was then advanced into the left ventricle to measure the following parameters (*figure 10*): left ventricular systolic (LVSP)and end-diastolic pressure (LVEDP), the maximum rate of ventricular pressure rise ($+dP/dt_{max}$) and reduction ($-dP/dt_{max}$), taken as indexes of myocardial mechanical efficiency, isovolumic contraction time (IVCT: duration of isovolumic contraction), and total cycle duration (Tcycle) (software package AcqKnowledge 3.9; Biopac Systems, Goleta, CA).

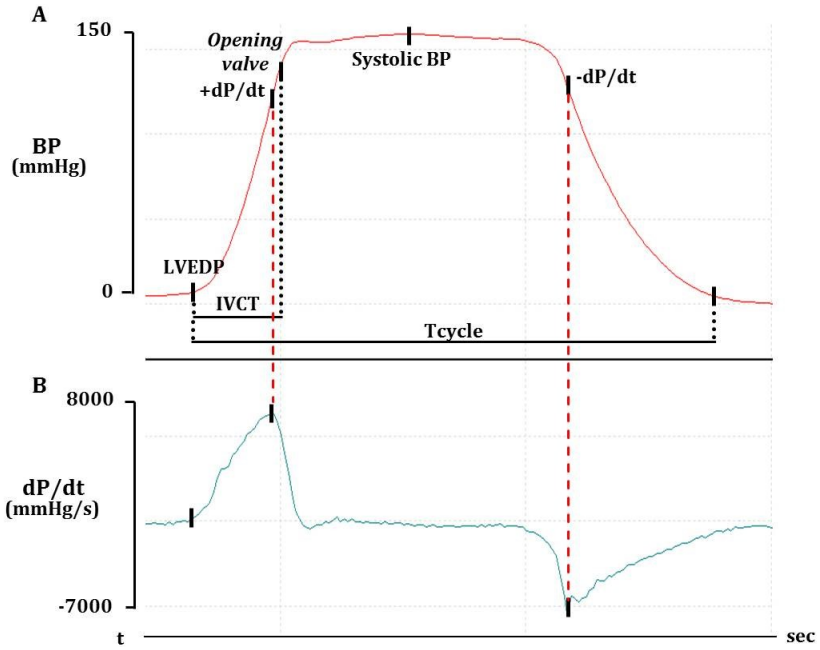

Figure 10. Schematic representation of a contractile event (**A**) and its relative first derivate (**B**) showing the measured parameters.

3.5 Isolation of adult LV cardiomyocytes

From the heart of each animal, individual left ventricle myocytes were enzymatically isolated by collagenase perfusion. The animals were anesthetized and after decapitation the heart was rapidly excised through median sternotomy and mounted on a Langendorff isolated heart apparatus.

The heart was then perfused at 37°C by cannulating the aorta with the following sequence of solutions gassed with 100% oxygen: (1) calcium-free solution for 5 min to remove the blood, (2) low-calcium solution (0.1 mM) plus 1 mg/ml type 2 collagenase (Worthington Biochemical Corporation, Lakewood, NJ, USA) and 0.1 mg/ml type XIV protease (Sigma-Aldrich) for about 15 min, and (3) an enzyme free, low-calcium solution for 5 min. Calcium-free solution contained the following (in mM, all chemicals from Sigma-Aldrich): 126 NaCl, 22 dextrose, 5.0 $MgCl_2$, 4.4 KCl, 20 taurine, 5 creatine, 5 Na pyruvate, 1 NaH_2PO_4, and 24 HEPES (pH = 7.4, adjusted with NaOH).

Once completed the enzymatic digestion, the heart was removed from the perfusion apparatus and then the left ventricle was minced and shaken for 10 min. The cells were filtered through a nylon mesh and a fraction was re-suspended in low-calcium solutions for 20 min, gradually brought to 1mM Ca^{2+} in about 80 minutes, and then used for measuring sarcomere shortening and calcium transients.

3.6 Cardiomyocyte contractility and Ca^{2+} transients

Mechanical properties and calcium transients were recorded by using the IonOptix fluorescence and contractility systems (IonOptix, Milton, MA, USA). Left ventricle myocytes were placed in a chamber mounted on the stage of an inverted microscope (Nikon-Eclipse TE2000-U, Nikon Instruments, Florence, Italy, *figure 11*) and superfused (1 mL/min at 37°C) with a Tyrode solution containing (in mM, all chemicals from Sigma-Aldrich): 140 NaCl, 5.4 KCl, 1 $MgCl_2$, 5 HEPES, 5.5 glucose, and 1 $CaCl_2$ (pH 7.4, adjusted with NaOH).

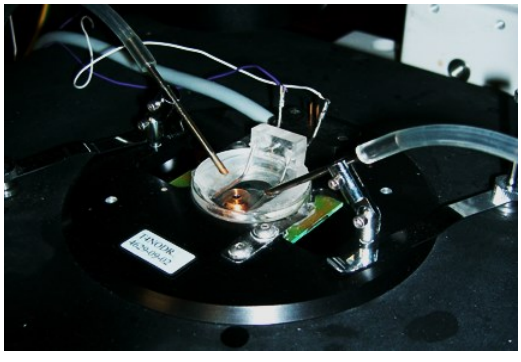

Figure 11. Stimulation/perfusion thermostated chamber mounted on the stage of an inverted microscope.

Only rod-shaped myocytes with clear edges and average sarcomere length ≥ 1.7 μm were selected for the analysis, using a 40X oil objective lens (NA:1.3). None of the

selected myocytes showed spontaneous contractions. The cells were field-stimulated at a frequency of 0.5 Hz and 1Hz by constant current pulses (2 ms in duration, and twice diastolic threshold in intensity; MyoPacer Field Stimulator, IonOptix), delivered by platinum electrodes placed on opposite sides of the chamber, connected to a MyoPacer Field Stimulator (IonOptix). The stimulated myocyte was displayed on a computer monitor using an IonOptix MyoCam camera. Load-free contraction of myocytes was measured with the IonOptix system, which captures sarcomere length dynamics via a Fast Fourier Transform algorithm. Cardiomyocyte contractile properties and calcium dynamics were simultaneously recorded in LV myocytes (*figure 12*).

Ca^{2+} transients were detected by epifluorescence after loading the myocytes with Fluo-3 AM (5 μM; Thermo Fisher Scientific, Waltham, MA, USA), previously mixed with PluronicTM F-127 (10% final concentration; Thermo Fisher Scientific, Waltham, MA, USA), for 20 min. Excitation length was 480 nm, with emission collected at 535 nm. The steady-state contraction of myocytes was achieved before data recording by means of a 10 s conditioning stimulation. The sampling rate was set at 1 kHz.

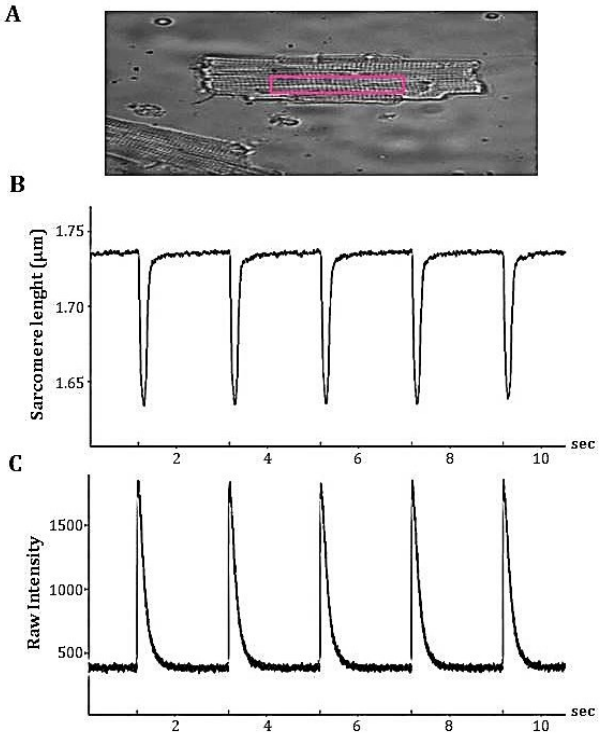

Figure 12. Cardiomyocyte framed with the IonOptix hardware/software system (A), representative traces of sarcomere shortening (B) (each deflection corresponds to the mean sarcomere shortening included in the fuchsia rectangle), and corresponding Ca^{2+} transients (C).

A total of 682 isolated ventricular myocytes were analysed: 216 cells from EXP.1a (82 CTRL and 134 GTE), 216 cells form EXP.1b (66 CTRL, 72 GTE, and 78 EGCG), and 170 cells from EXP.2 (59 CTRL, 56 D3, and 55 D3_GTE).

From the mean sarcomere shortening trace the following parameters were computed (*figure 13)*:

- mean diastolic sarcomere length (BL);
- fraction of shortening (FS);
- maximal rates of shortening ($-dl/dt_{max}$) and re-lengthening ($+dl/dt_{max}$);
- time to 10, 50, and 90% of re-lengthening (RL10%, RL50%, and RL90%).

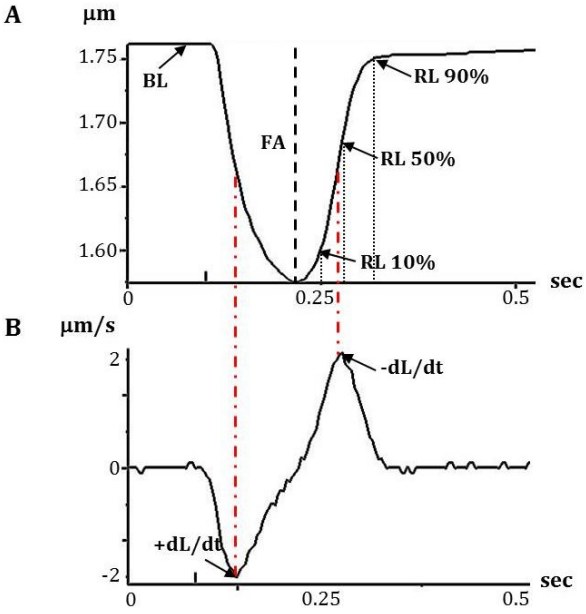

Figure 13. Schematic representation of mean sarcomere shortening track (A) and its relative first derivate (B) showing the measured parameters.

Fluo 3 signals were expressed as normalized fluorescence (f/f0: fold increase, *figure 14*). The time course of the fluorescence signal decay was described by a single exponential equation, and the time constant (tau) was used as a measure of the rate of intracellular calcium clearing.

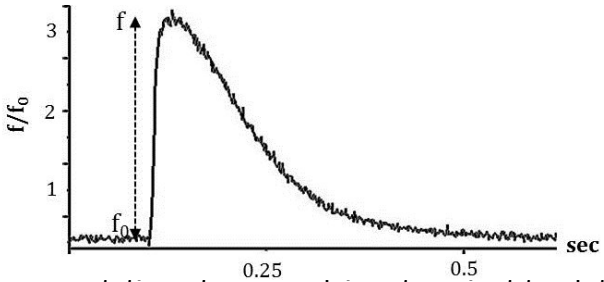

Figure 14. Schematic representation of mean calcium transient track that was normalized and expressed as fold increase.

3.7 Respiration rate measurements

Respiratory rates of left ventricular myocytes isolated from the hearts of control, GTE, and EGCG- rats, were assayed polarographycally at 30°C using a Clark-type oxygen electrode. Mitochondrial respiration was determined in intact cells suspended in the isolation buffer (low calcium solution, 0.1mM), containing 22 mM glucose and 5 mM pyruvate as energy substrates. The endogenous respiration was sensitive to rotenone and antimycin A. The oxygen consumption rate was also measured in permeabilized cardiomyocytes (60 μg/ml of digitonin,1.5 x 10^5 cells/ml) suspended in a buffer containing in mM: 250 sucrose, 20 Tris/Cl, 4 $MgSO_4$, 0.5 EDTA, and 10 KH_2PO_4, pH 7.4. Under state 3 conditions, the NADH dependent-oxygen consumption was measured at 30°C (saturating oxygen concentration is 204.1 μM) by adding 10 mM glutamate, 10 mM malate (plus 1.8 mM malonate), and 0.5 mM ADP as substrates. The state 4 respiration rate was measured following the addition of 1 μM oligomycin. We calculated the initial rate of respiration under both state 3 and state 4 conditions by evaluating the oxygen concentration decline during the first two minutes reaction of each state. The respiratory control ratio (RCR) was defined as the State 3/State 4 respiratory rates ratio. Cells were counted by using the MUSE cell analyzer (Millipore, Billerica, MA, USA), and the respiration rates were expressed as nmol/min/10^6 cells.

3.8 Citrate synthase activity assay

The citrate synthase activity of rat cardiomyocytes was detected by incubating 1.5 x 10^3 cells in 1 ml of 0.125 M Tris-HCl, 0.2% triton, 0.1 mM acetyl-coenzyme A, 0.1 mM 5,5'-dithio-bis (2-nitrobenzoic acid) (DTNB), and 0.5 mM oxaloacetate. The activity was assessed by monitoring the release of 2-nitro-5-thiobenzoate (ε = 13.6 mM-1cm-1) at 412 nm and was expressed as μmol/min/10^6 cells.

3.9 ATP content analysis in isolated LV cardiomyocytes

The intracellular content of ATP was measured by the Luminescence ATP Detection Assay System (ATPlite; PerkinElmer, Waltham, MA, USA) according to the manufacturer's protocol. A frozen pellet of isolated left ventricular cardiomyocytes was re-suspended in 1 mL of PBS and 20 μL of this suspension was further diluted to a final

volume of 400 µL with PBS. Aliquots of 100 µL of diluted cell suspension were pipetted in triplicate in a 96-well white plate. Then, 50 µL/well of mammalian cell lysis solution were added and the plate was shaken at 700 rpm for 5 minutes in an orbital shaker before to add 50 µL/well of substrate solution. The microplate was shaken again for 5 minutes and dark incubated for 10 minutes. The luminescence intensity was then measured by the EnSpire® multimode plate reader (PerkinElmer). The row luminescence data, given in relative light units (RLU), were normalized for the total protein content of each sample, measured by the DC Protein assay kit (Bio-Rad, Hercules, CA, USA).

3.10 Protein extraction, SDS–polyacrylamide gel electrophoresis (SDS-PAGE), and western blot (WB) analysis

Left ventricle tissues of 8 rats from EXP.1a (4 CTRL and 4 GTE) and 8 from EXP.1b (3 GTE, 3 EGCG, and 2 CTRL) were finely ground in liquid nitrogen. Thirty mg of powder were homogenized in 500 µL of ice-cold modified RIPA buffer (50 mM Tris- HCl pH 7.4, 100 mM NaCl, 1% Triton X-100) supplemented with adequate amount of protease and phosphatase inhibitor cocktails (Sigma-Aldrich). In addition, ice-cold RIPA buffer plus inhibitors was used to lyse isolated cardiomyocytes. Extracts were centrifuged (14000 rpm for 30 min at 4°C) and supernatants were stored at -20°C. Protein concentration was estimated by the DC Protein assay kit (Bio-Rad) using bovine serum albumin (Sigma-Aldrich) as a standard. The equivalent of 75 µg of total lysate was incubated for 30-40 minutes at 37°C before being loaded and resolved by 15% acrylamide SDS-PAGE. For western blot analysis, proteins were electrophoretically transferred, overnight at 4°C, to PVDF membranes (EMD Millipore, Merk KGaA, Darmstadt, DE). Transfer efficiency was routinely monitored by 0.1% Ponceau S staining (Sigma-Aldrich).

For the analysis of SERCA2, PLB, and p-PLB expression, blotted membranes were incubated with TBS-T buffer (50 mM Tris-HCl pH 7.5, 150 mM NaCl, 0.1% Tween 20) containing 5% (w/v) non-fat dry milk powder for 3 or 6 hours at room temperature with gentle shaking. Membranes were probed overnight at 4°C with the primary antibodies diluted in TBS-T containing 5% (w/v) non-fat dry milk. The following antibodies were used: rabbit polyclonal anti-phospho-Phospholamban (Ser16), dilution 1:200, from Millipore (EMD Millipore Corporation, Temecula, CA); mouse monoclonal

anti-Phospholamban (2D12), dilution 1:1000; rabbit polyclonal anti-SERCA2 ATPase, dilution 1:1000, from Abcam (Cambridge, UK); mouse monoclonal anti-β actin, dilution 1:500, from Santa-Cruz Biotechnology (Santa Cruz, CA, USA).

For the analysis of OXPHOS complexes were used the following antibodies: mouse monoclonal anti-NADH ubiquinone oxidoreductase subunit A9 (anti-NDUFA9, dilution 1: 1000) for Complex I; mouse monoclonal anti-succinate dehydrogenase complex flavoprotein subunit A (anti-SDHA, dilution 1:2500) for Complex II; mouse monoclonal anti-ubiquinol cytochrome c reductase core protein (anti-UQCRC2, dilution 1:1000) for Complex III; mouse monoclonal anti-cytochrome c oxidase subunit I (anti- COX-I, dilution 1:1000) for Complex IV; mouse monoclonal anti-ATP synthase F_1 subunit alpha (anti-ATP5A, dilution 1:2000) and anti-ATP synthase F_1 subunit d (anti- ATP5H, dilution 1:1000) for Complex V; anti-translocase of the outer mitochondrial membrane 20 (TOMM20, dilution 1:1000). All the antibodies were purchased from AbCam (Cambridge, UK).

After extensive washes with TBS-T, membranes were incubated with horseradish peroxidase-conjugated anti-mouse (dilution 1:5000) or anti-rabbit (dilution 1:200000) secondary antibodies (Sigma-Aldrich) diluted in TBS-T containing 5% (w/v) non-fat dry milk for 1 hour at room temperature.

Immunoreactive bands were detected using the BM Chemiluminescence Western Blotting Substrate (Hoffmann-La Roche, Basel, Switzerland) and quantified by the Quantity Basic analysis software (BioRad).

3.11 RNA extraction, retrotranscription, and RT-qPCR analysis

GTE and CTRL ventricles were ground in liquid nitrogen to a fine powder. About 10 mg of powder were dissolved in 1 mL of TRIZOL reagent (Thermo Fisher Scientific, Waltham, MA, USA), purified with the PureLink RNA Mini kit (Thermo Fisher Scientific) and reverse transcribed using the RevertAid First Strand cDNA Synthesis kit (Thermo Fisher Scientific) according to the manufacturer's instructions. For each sample 250 ng of total purified RNA was combined with 1 µL of Oligo dT Primers (100 µM) and heated at 65°C for 5 min. After a quick chilling on ice, the first strand synthesis reaction was carried out for 60 min at 42°C and stopped at 70°C for 5 min. Two µL of each cDNA obtained, diluted 1:2 in water, were used for RT-qPCR amplification by the SSOAdvanced

Universal SYBR Green Supermix (Bio-Rad) and performed in duplicate on the DNA Engine Opticon 4 (MJ Research, Walthman, MA, USA). Thermal cycler conditions consist of an initial denaturation at 95 °C for 30 seconds followed by 40 cycles of denaturation at 95 °C for 15 seconds and annealing and extension at 60 °C for 20 seconds.
The set of primers (10μM final concentration) used for the RT-qPCR analysis are shown in the following table:

Gene	Forward primer sequence 5' 3'	Reverse primer sequence 5' 3'	Ref.
GAPDH	GTTCCAGAGACAGCCGCATC	CGTTCACACCGACCTTCACC	Prasad AM, 2011
PLN	CATGCCAACGCAGTTACAACCT	TCGTGACCCTTCACGACGAT	Prasad AM, 2011
NCX1	CGAAATGGATGGGAAAGTAGTCAAC	TCTTTGTCGGGATGCTTCTGC	Prasad AM, 2011
SERCA	AACTACCTGGAGCCTGCAAT	TTCCCCAAGCTCAGTCATGC	
CACNA1C	ATGGTTCTTGTCAGCATGTTGCGG	TGCAAATGTGGAACCGGTGAAGTG	Hui K, 2013
RYR2	GGCGGAATTTCTTGCCAAC	CCTCGCACCTCATCCTGAGT	
PGC-1α	GTGCAGCCAAGACTCTGTATGG	GTCCAGGTCATTCACATCAAGTTC	Valian N, 2017
NRF1	AAATTGGGCCACATTACAGGG	GTTGCATCTCCTGAGAAGCG	Rehman H, 2014
TFAM	AGAGTTGTCATTGGGATTGG	CATTCAGTGGGCAGAAGTC	Rehman H, 2014

Table 1. Primer sequences.

Primer pair for SERCA2 was designed using the NM_001110139.2 GenBank sequence by means of PrimerBLAST (NCBI; www.ncbi.org/bast/primerblast). RYR2 primers were freely accessible in RTPrimerDB database (http://www.rtprimerdb.org).
qPCR data analysis was performed by calculating the cycle threshold (Ct), that is the number of cycles required for the fluorescent signal to cross the threshold, for each gene. Row Ct values of target genes were normalized for the Ct value of the reference gene glyceraldehyde phosphate dehydrogenase (GAPDH) measured in the same sample, according to the following equation: normalized Ct (ΔCt) = $Ct_{\text{target gene}} - Ct_{\text{GAPDH}}$.

3.12 DNA extraction and relative quantification of the mtDNA content

Total DNA was extracted from GTE, EGCG, and CTRL left ventricle by using the commercial Kit NucleoSpin Tissue (Macherey-Nagel, Duren, Germany) according to manufacturer's instructions and quantified by a Biospectrophotometer (Eppendorf AG, Germany). Then, 0.1 ng of DNA, quantified by the QuantiFluor ONE System using the

Quantus Fluorometer (Promega Corporation, Madison, USA), was used for qPCR amplification by the SSO-Advanced Universal SYBR Green Supermix (Bio-Rad). Mitochondrial DNA (mito gene) corresponding to sequences of the NADH-ubiquinone oxidoreductase subunit 1, the NADH-ubiquinone oxidoreductase subunit 3 and the displacement loop region of mitochondrial DNA were amplified using the primers set (10μM final concentration) shown in *table 2*. The GAPDH gene was used as a nuclear DNA marker (nucl gene).

Gene	Forward primer sequence 5' 3'	Reverse primer sequence 5' 3'	Ref.
GAPDH	GTTCCAGAGACAGCCGCATC	CGTTCACACCGACCTTCACC	Prasad AM, 2011
ND1	TTAATTGCCATGGCCTTCCTCACC	TGGTTAGAGGGCGTATGGGTTCTT	Nicklas JA, 2004
ND3	CAACAAGTTCTGCACGCCTTCCTT	TTGTTTGAATCGCTCATGGGAGGG	Rehman H, 2014
D-loop	GGTTCTTACTTCAGGGCCATCA	GATTAGACCCGTTACCATCGAGAT	Nicklas JA, 2004

Table 2. Primer sequences.

We used the Basic Local Alignment Search Tool (BLAST) software (from NCBI) to identify those primers that specifically recognized unique mtDNA sequences in order to avoid amplification of nuclear mitochondrial insertion sequences (pseudogenes) that might negatively affect accurate mtDNA quantification.

Thermal cycler conditions consisted of an initial denaturation at 95 °C for 30 seconds, followed by 40 cycles of denaturation at 95 °C for 15 seconds, and annealing and extension at 60 °C for 20 seconds. To calculate the relative mtDNA content, the following equations were used:

$$\Delta Ct = Ct_{\text{nucl gene}} - Ct_{\text{mito gene}}$$

$$\text{Relative mtDNA content} = 2x2^{\Delta Ct}$$

3.13 Ultrastructural analysis of LV myocardium by TEM

Fresh left ventricle samples were fixed in Karnovsky, washed several times with phosphate buffer (0.1 M, pH 7.2), and post-fixed for 90 minutes at RT in 1% osmium tetroxide (OsO_4). Following dehydration achieved by increasing the concentration of alcohol, samples were washed with propylene oxide and embedded in epoxy resin. Sections of 0.5 μm thickness were stained with methylene blue and safranin to morphologically select the field of interest. Subsequently, ultrathin sections of 60–80 nm

thickness were collected on a 300-mesh copper grid, and stained with uranyl acetate and lead citrate. Sections were qualitatively examined under a transmission electron microscope (Philips EM 208S; Fei Electron Optics BV, Eindhoven, Netherlands).

3.14 Statistical analysis

The IBM SPSS statistical package (International Business Machines Corporation, Armonk, NY, USA, version 25) was used. Normal distribution of variables was checked by means of the Kolmogorov–Smirnov test. Data are expressed as mean values ± standard error of the mean (SEM). Comparisons among groups involved unpaired Student's t test (hemodynamics), GLM ANOVA for repeated measurements (cell mechanics, calcium transients, and intracellular ATP levels) followed by Sidak post-hoc test, one-way ANOVA followed by the Bonferroni's post-hoc test (mitochondrial respiration rates), non-parametric statistical test U-Mann Whitney (western blot data and RT-qPCR data EXP.1a), and non-parametric Median test (mtDNA content, mitochondrial biogenesis and protein expression EXP.1b). Differences were considered statistically significant at $p < 0.05$.

4. RESULTS of the EXPERIMENTAL PROTOCOL 1a

[Bocchi L, 2018]

4.1 Body weight

The body weights measured at the beginning of the experimental protocol were comparable between CTRL and GTE groups and exhibited only minor changes during the following four weeks. No significant differences were observed between the two experimental groups, at all the time points considered (*table 3*).

	CTRL	GTE
Day 0	414.7 ± 12.2	417.8 ± 11.4
Day 7	423.4 ± 8.8	402.3 ± 14.5
Day 14	432.6 ± 7.8	412.0 ± 13.9
Day 21	437.8 ± 7.2	415.4 ± 15.2
Day 28	441.1 ± 7.4	422.3 ± 15.7

Table 3. Mean values ± SEM of body weights (g) measured once a week in untreated (CTRL) and treated (GTE) animals.

4.2 Hemodynamic study

The heart rate measured under anaesthesia did not show substantial differences between GTE and CTRL animals (range 185-251 beats/min in CTRL, 195-276 beats/min in GTE rats). No significant differences were observed in the average values of most parameters between the experimental groups, other than the maximal rate of left ventricular pressure decline during isovolumic relaxation ($-dP/dt_{max}$), significantly increased in GTE treated rats (+15%, *table 4*).

	CTRL	GTE
Systolic arterial BP (mmHg)	131.9 ± 4.89	134.4 ± 4.39
Diastolic arterial BP (mmHg)	103.5 ± 2.15	104.7 ± 2.96
LVSP (mmHg)	138.5 ± 5.75	138.6 ± 5.58
LVEDP (mmHg)	5.60 ± 0.41	4.62 ± 0.37
$+dP/dt_{max}$ (mmHg/s)	7358.2 ± 222.7	7368.6 ± 183.6
$-dP/dt_{max}$ (mmHg/s)	-6605.1 ± 269.1	-7592.4 ± 263.2 *
IVCT (s)	0.021 ± 0.0004	0.021 ± 0.0006
Tycle (s)	0.140 ± 0.006	0.138 ± 0.005

Table 4. Hemodynamic measurements. Mean values ± SEM of systolic arterial blood pressure (BP), diastolic arterial BP, left ventricular systolic pressure (LVSP), left ventricular end diastolic

pressure (LVEDP), maximal rate of LV pressure rise (+dP/dtmax), maximal rate of LV pressure decline (-dP/dtmax), isovolumic contraction time (IVCT), and total cycle duration (Tcycle), measured in control rats (n=10) and GTE rats (n=10). * $p<0.05$ vs CTRL.

4.3 Cardiomyocyte mechanics and Ca^{2+} transients

The analysis of mechanical properties revealed that in the absence of marked changes in the average diastolic sarcomere length (BL, *figure 15C*), GTE cardiomyocytes exhibited a significant increase in the fraction of shortening (FS, *figure 15D*) and the maximal rate of shortening (-dl/dt_{max}, *figure 15E*) and re-lengthening (+dl/dt_{max}, *figure 15F*), resulting in shorter relaxation times measured at 10% and 50% of re-lengthening (RL10% and RL50%, *figure 15G*). In accordance with mechanics data, an improved efficiency of the mechanisms involved in the intracellular calcium handling was observed in GTE group, as documented by the higher amplitude of the calcium transient (f/f0, *figure 15H*), associated with lower values of *tau* (tau, *figure 15I*), denoting a faster cytosolic calcium removal.

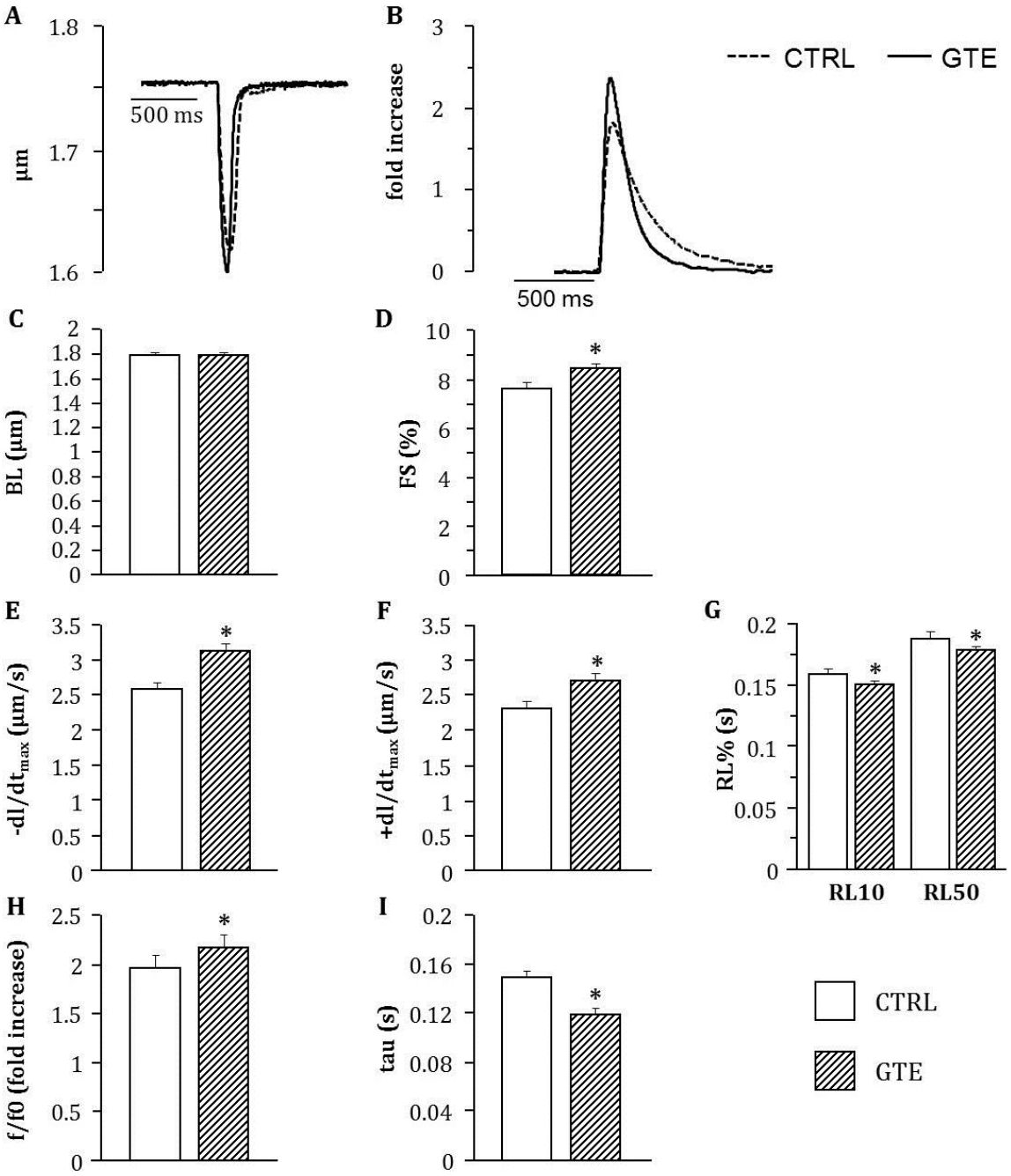

Figure 15. Effects of GTE administration on cell mechanics and calcium transients in cardiomyocytes isolated from adult rat hearts. Representative examples of sarcomere shortening (**A**) and corresponding calcium transients (**B**; normalized traces: fold increase) recorded from CTRL (dashed line) and GTE (solid line) ventricular myocytes. In **C-I** bar graphs, means values ± SEM of: mean diastolic sarcomere length (BL; **C**), sarcomere fraction of shortening (FS; **D**), maximal rate of shortening ($-dL/dt_{max}$; **E**), maximal rate of re-lengthening ($+dL/dt_{max}$; **F**), time to 10 and 50% of re-lengthening (RL10%, RL50%; **G**), calcium transient amplitude expressed as peak fluorescence normalized to baseline fluorescence (f/f0; **H**), and time constant of the intracellular calcium decay (tau; **I**), measured in CTRL (82 cells) and GTE (134 cells).* $p<0.05$ significant differences vs CTRL.

4.4 ATP content analysis in LV cardiomyocytes

In order to explain, at least in part, the higher contractile efficiency observed in GTE cells we evaluated the total intracellular ATP content. The ATP availability was significantly increased in GTE cardiomyocytes as compared with CTRL (+25%, *figure 16*). Local energetic control is essential not only for the functioning of the two major ATPases implicated in the contraction and relaxation processes, i.e. SERCA2 and the myosin ATPase, but also for the efficient function of myofibrils. Moreover, changes in ATP content are associated with parallel variations in cardiomyocyte ATPase activity, [Joubert F, 2008; Kuum M, 2009].

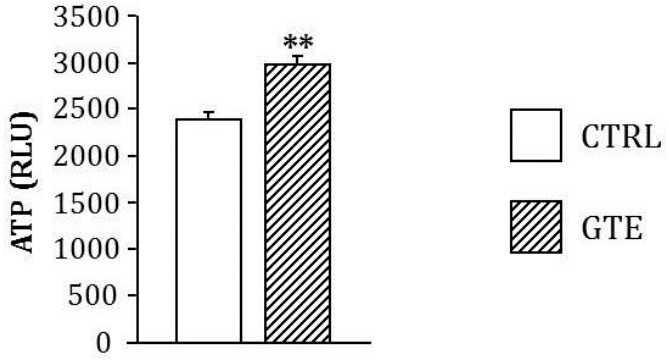

Figure 16. Effects of GTE supplementation on left ventricle myocytes ATP content. Mean values ± SEM of ATP content in CTRL and GTE cardiomyocytes. Values are expressed as relative light units (RLU) normalized to the protein content. ** $p<0.001$ vs CTRL.

4.5 Electrophoresis and western blot analysis of SERCA2, PLB, and p-PLB

To understand the potential molecular mechanisms responsible for the improved cardiomyocyte contractility and calcium dynamic observed in GTE rats, we evaluated SERCA2, PLB, and p-PLB expression levels. In cardiac tissue, SERCA2 plays a central role in regulating the intracellular calcium handling and thus controlling excitation/contraction coupling. Indeed, SERCA2: (i) promotes cardiac relaxation by pumping calcium ions from the cytosol into sarcoplasmic reticulum (SR) lumen and, at the same time, (ii) restores SR calcium store necessary for contraction [Frank KF, 2003]. The Ca^{2+} pump activity in cardiac SR is reversible regulated by a small molecular weight protein, the phospholamban. Specifically, the phosphorylation status of PLB is able to remove the inhibitory effect of PLB on SERCA2, increasing Ca^{2+} uptake in the SR and enhancing myocyte contractility and relaxation [Eisner DA, 2017]. Western blot analysis

showed that the SERCA2 expression levels were comparable in CTRL and GTE (*figure 17A*). Conversely, in GTE was observed a marked decrease in the total PLB levels (-23%, p=0.08, *figure 17B*) associated with an increase in the phosphorylated form of the protein (+58%, p=0.08, *figure 17C*), leading to a significant increase in the p-PLB/PLB ratio (*figure 17D*). On the other hand, we found that the SERCA/PLB ratio was significantly increased in GTE hearts in comparison to CTRL (+15%, *figure 17E*). A SERCA2/PLB ratio increase was shown to be associated with a parallel enhanced SERCA2 affinity for Ca^{2+} and may further contribute to improve the mechanical efficiency of GTE-treated cardiomyocytes [Pattison JS, 2008].

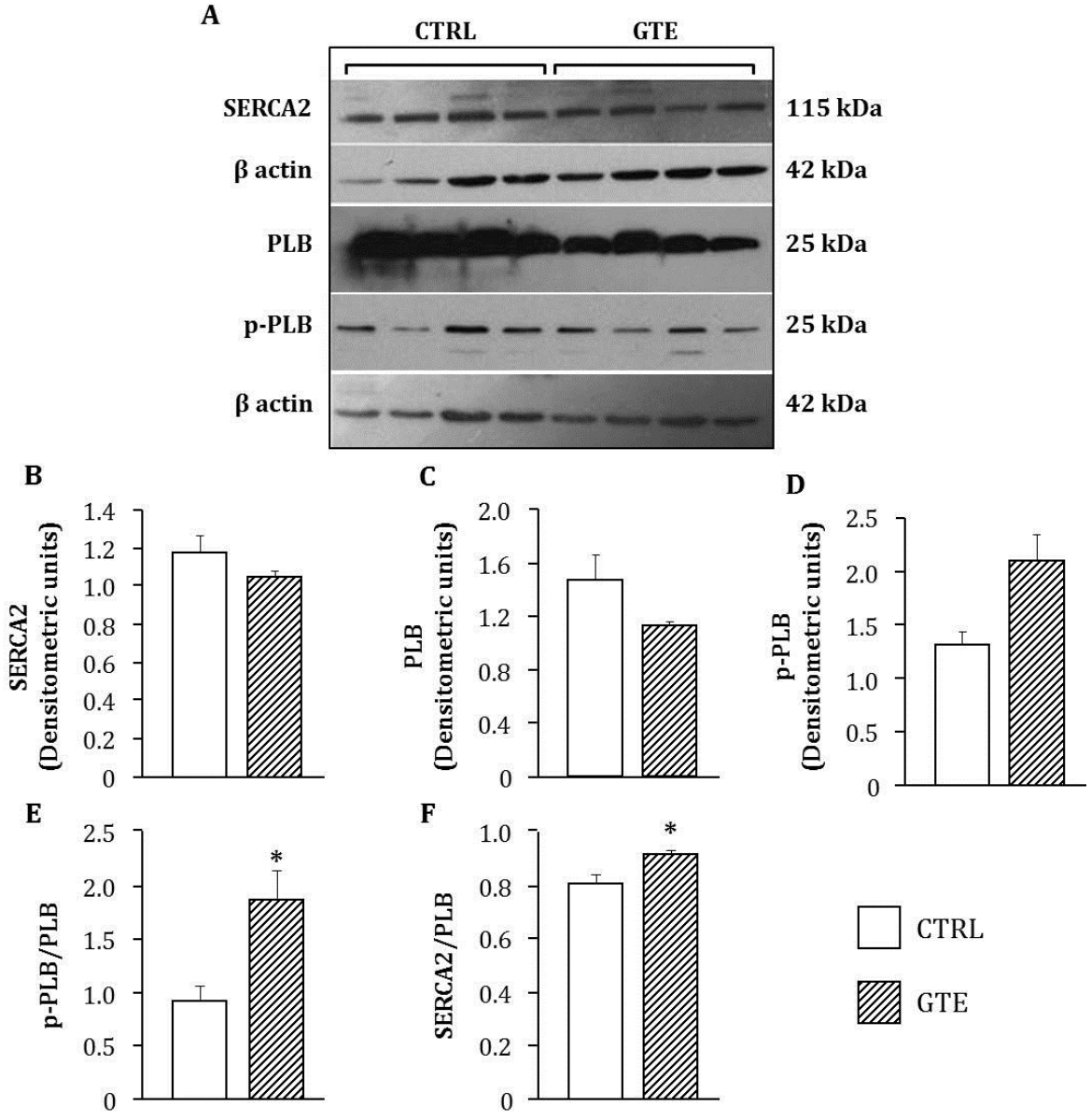

Figure 17. Expression levels of functional proteins by immunoblot assay. **A:** sets of bands related to SERCA, PLB, p-PLB, and β actin expression, in CTRL (n=4) and GTE (n=4) left

ventricular myocardium. Mean values ± SEM of SERCA2 (**B**), PLB (**C**), and p-PLB (**D**) expression levels normalized to β-actin, measured by densitometric analysis. In **E** and **F** are reported p-PLB/PLB ratio and SERCA2/PLB ratio, respectively. * $p<0.05$ significant differences vs CTRL.

4.6 RNA extraction, retrotranscription, and RT-qPCR analysis

In order to investigate the effects of GTE on gene expression of cardiac ion channels, as well as regulatory and functional proteins involved in the excitation-contraction coupling, we performed a RT-qPCR assay. We measured the steady state levels of mRNA encoding the subunits of SERCA2 and its major regulatory protein PLB, the sodium calcium exchanger, the voltage dependent L-type calcium channel, and ryanodine receptor. As observed at the protein level, the expression of SERCA2 and PLB mRNA were comparable in CTRL and GTE (*figure 18*). Furthermore, GTE did not influence the gene expression of CACNA1C, NCX1, and RYR2 measured in the left ventricular samples, in comparison with controls.

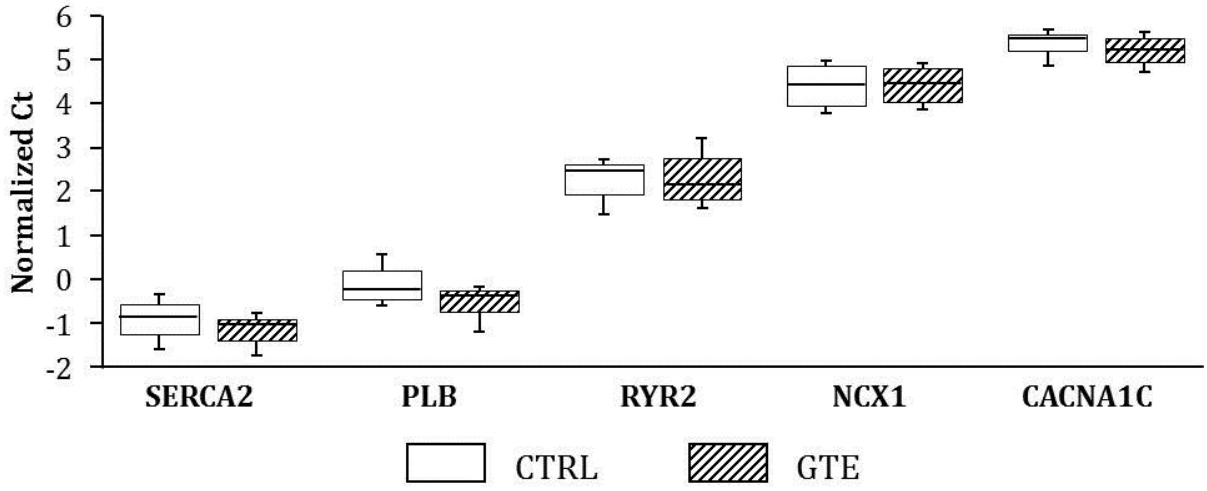

Figure 18. Effects of GTE on gene expression evaluated by RT-qPCR. Box plot distribution of the Ct values of SERCA2, PLB, RYR2, NCX1, and CACNA1C, normalized to the Ct of GAPDH measured in ventricular tissue samples of CTRL (n=4) and GTE (n=4) groups. A higher normalized Ct value means lower gene expression levels. Negative Ct values mean that the target gene is more expressed than GAPDH.

5. RESULTS of the EXPERIMENTAL PROTOCOL 1b

[Vilella R, 2020]

5.1 Body weight

The body weights of each animal were checked weekly and before sacrifice. As shown in the *table 5*, a small increase in the body weight, about 3%, was observed in all the animals over the course of the experiment. No significant differences were found among the three experimental groups at all time points.

	CTRL	GTE	EGCG
Day 0	423.2 ± 5.9	426.0 ± 16.4	427.2 ± 10.8
Day 7	428.4 ± 7.5	426.0 ± 16.9	425.2 ± 12.9
Day 14	431.4 ± 9.4	434.6 ± 19.2	436.0 ± 10.3
Day 21	430.8 ± 11.6	435.6 ± 15.9	441.8 ± 10.7
Day 28	437.0 ± 9.6	441.4 ± 21.2	441.2 ± 7.9

Table 5. Mean values ± SEM of body weights (g) measured once a week in untreated (CTRL), GTE, and EGCG treated rats.

5.2 ATP content analysis in LV cardiomyocytes

To verify whether the increase in the ATP content measured after long-term *in vivo* GTE oral administration in EXP.1a could be due to its major component, epigallocatechin-3-gallate, we evaluated the effect of GTE and EGCG on cardiomyocyte ATP levels. A significant increase in ATP intracellular content was measured in both GTE (+25%) and EGCG (+16%) compared with CTRL (*figure 19*). No statistically significant differences were observed between the two treated groups.

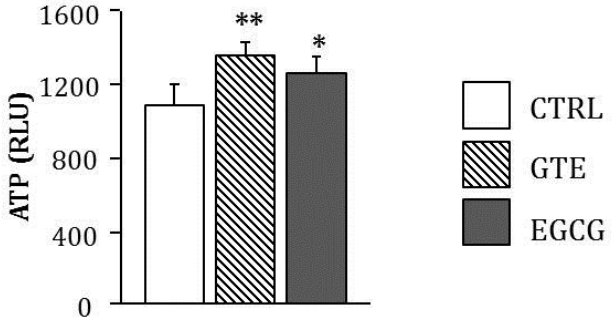

Figure 19. Effects of GTE and EGCG on cardiomyocyte ATP content. Mean value ± SEM of ATP content in CTRL, GTE, and EGCG left ventricle myocytes. Values are expressed as relative light units (RLU) normalized to the protein content. * $p<0.05$, ** $p<0.01$ vs CTRL.

5.3 Mitochondrial respiration and citrate synthase activity in LV cardiomyocytes

To evaluate the effect of GTE and EGCG administration on mitochondria function, we assayed the oxygen endogenous consumption rate of freshly cardiomyocytes isolated from GTE and EGCG treated rats (*figure 20A-C*). A significant increase in the respiration rate was observed in both GTE and EGCG cardiomyocytes as compared to controls (+24% and +18% respectively, *figure 20C*).

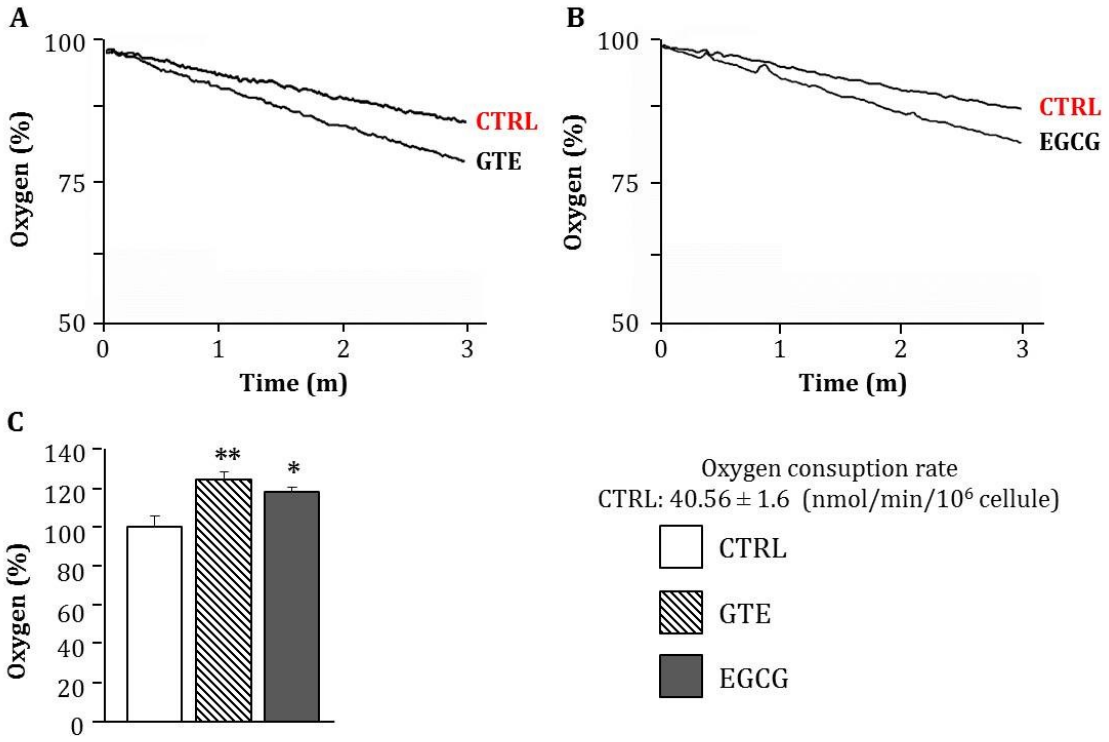

Figure 20. GTE and EGCG administration affects rat cardiomyocyte mitochondrial respiration. **A-B**: typical oxygen consumption traces in GTE (**A**) and EGCG (**B**) intact cells compared to CTRL. Oxygen concentration at 30°C is 204.1 µM (100 % saturation). In **C** bar graph, mean values ± SEM of the oxygen consumption rate percentage changes of treated cells as compared with CTRL cardiomyocytes. * $p<0.05$ and ** $p<0.01$ indicate the statistical significance of data compared to controls.

In addition, we performed complex-I-dependent respiration measurements in permeabilized left ventricle myocytes under both state 3 and state 4 respiration conditions by adding glutamate/malate as energizing substrate in presences of ADP (state 3) and upon the oligomycin-induced ATP synthase inhibition (state 4) (*figure 21A*). The state 3 respiration rate was significantly increased (+25%) in both GTE and

EGCG cardiomyocytes compared to controls (*figure 21B*), indicating that both treatments significantly enhanced the cardiomyocyte OXPHOS rate. Conversely, the state 4 respiration rate was similar among the three experimental groups. We also evaluated the respiratory control ratio (i.e. the state3 to state4 respiratory rate ratio) that strictly depends on the functional integrity of the inner mitochondrial membrane and is considered an index of the OXPHOS efficiency. No significant changes of the RCR were observed in both GTE an EGCG treated rats compared to CTRL (*figure 21D*), suggesting that the energetic coupling between the respiratory chain and the ATP synthase activities was unchanged.

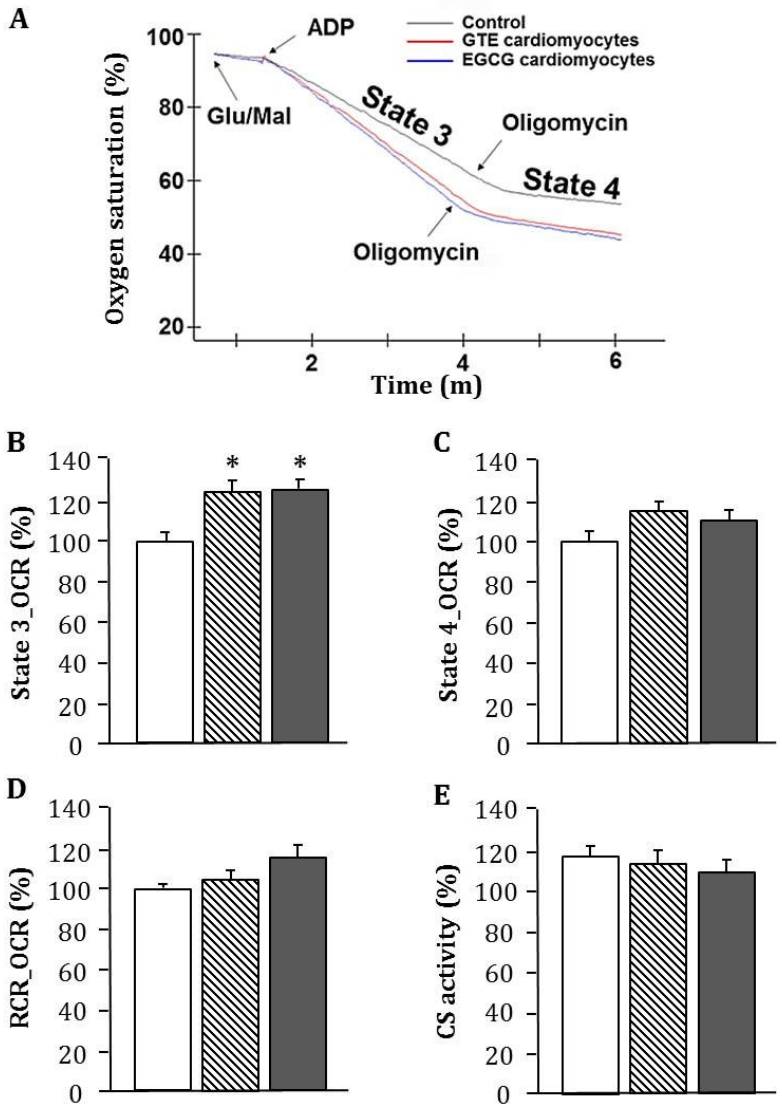

Figure 21. A: typical Complex I-driven oxygen consumption traces of permeabilized cardiomyocytes isolated from control rats (black line), GTE (red line) and EGCG (blue line) treated rats. In bar graphs **B-E**: mean values ± SEM of respiration rates under state 3 (**B**) and

state 4 (**C**), RCRs (state3/state4 respiration rate ratio; **D**), and the cytrate synthase activity reported as percent of controls (**E**). State 3 and state 4 rates of CTRL were 189.19 ± 10.37 and 41.38 ± 3.02 nmol/min/10^6 cells, respectively, RCR was 4.59 ± 0.14, and the cytrate synthase activity was 7.68 ± 0.30 μmol/min/10^6. * $p<0.05$ indicate the statistical significance of data compared to controls.

In order to verify whether the increase of the ADP-dependent respiration rate (state 3) detected in both GTE and EGCG-treated cardiomyocytes might be due to a mitochondrial mass increase, we assayed the activity of the citrate synthase (CS). CS is a tricarboxylic acids cycle enzyme located in the mitochondrial matrix and is used as a mitochondrial mass index [Costanzini A, 2019]. No significant changes of the CS activity were detected in both GTE and EGCG-treated cardiomyocytes compared to controls (*figure 21E*), suggesting that the increased state 3 respiration could be due to an augmented level and/or activity of the OXPHOS complexes.

5.4 Electrophoresis and western blot analysis of OXPHOS complexes

In order to evaluate the expression levels of OXPHOS complexes, western blot analysis was performed in both, lysate cardiomyocytes and left ventricle tissue (*figure 22A* and *22B*, respectively).

A specific subunit of each OXPHOS complex was identified by immunodetection and quantified by densitometric analysis. To estimate the relative protein content, each subunit band was normalized to the mitochondrial protein loading control TOMM20. Cardiomyocytes isolated from both GTE and EGCG treated rats showed a significant increase (about 30%) in all the OXPHOS complexes expression levels in comparison to control, with the exception of Complex I which was found to be nearly 50% higher in GTE cells (*figure 22C*). A significant increment of Complex I and Complex III was also observed in GTE left ventricle tissue (33% and 45%, respectively) compared to CTRL (*figure 22D*).

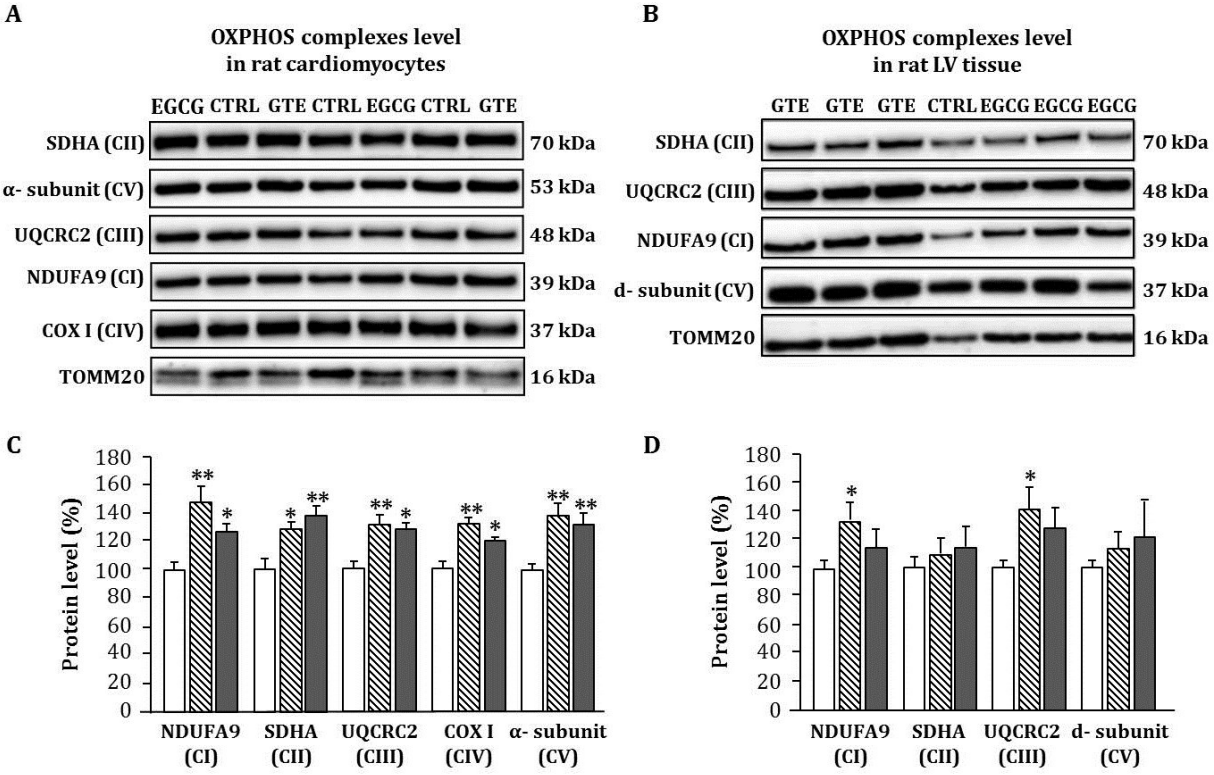

Figure 22. Effects of GTE and EGCG administration on OXPHOS complexes expression. Typical electrophoretic separation and immunodetection of OXPHOS complexes in cardiomyocyte (**A**) and LV tissue (**B**) lysates of CTRL, GTE and EGCG treated rats. The expression levels of specific subunit of each OXPHOS complex were measured by densitometric analysis in cardiomyocytes (**C**) and LV tissue (**D**) and normalized to TOMM20 protein level. Histograms show the mean ± SEM. * $p<0.05$ and ** $p<0.01$ indicate the statistical significance of data compared to controls.

5.5 Effects of GTE and EGCG on mtDNA content and mitochondrial biogenesis in rat LV tissue

The relative mtDNA content was measured in left ventricular tissue to assess the effect of GTE and EGCG on mitochondrial mass. Three distinct regions of the mitochondrial genome (ND1, ND3, and D-loop) were amplified. No significant reduction of mtDNA relative content was found in GTE and EGCG groups (-30% and -39% respectively) in comparison with controls (*figure 23A*), suggesting that the improvement of mitochondrial function observed in the treated cells occurred without a significant increase in the mitochondrial mass. Accordingly, the expression of genes involved in mitochondrial biogenesis measured in the same samples, was comparable in the three experimental groups (*figure 23B*).

Notably, the absence of important changes in mitochondrial mass following GTE and EGCG treatment, estimated in LV tissue by the mtDNA content and the quantification of transcription factors involved in mitochondrial biogenesis, was coherent with the observation carried out in isolated cardiomyocytes by evaluating the citrate synthase activity (*figure 21E*).

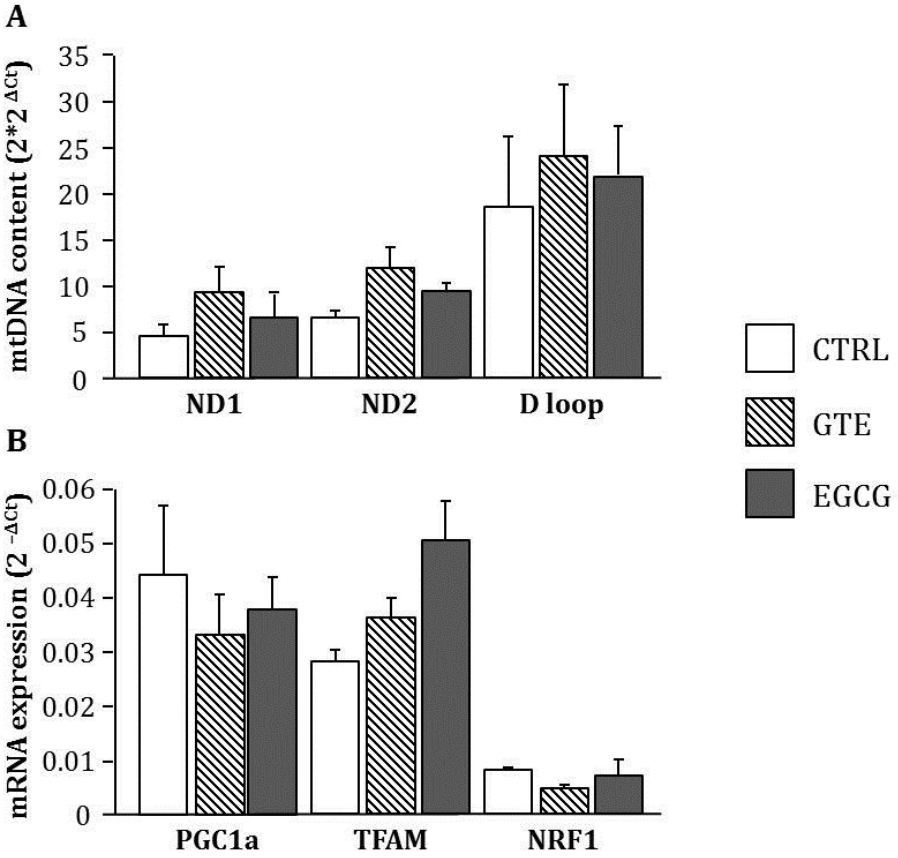

Figure 23. Effects of GTE and EGCG on ventricular tissue mtDNA content and mitochondrial biogenesis. (**A**) Relative mtDNA content of rat LV tissues. ND1, ND3, and D-loop region of the mtDNA were amplified and data were normalized to the content of nuclear DNA, estimated by GAPDH amplification. On the Y axis, 2*2ΔCt ± SEM has been reported, where ΔCt = Ct nucl gene – Ct mito gene. **(B)** Relative expression of genes involved in mitochondrial biogenesis (PGC1α, NRF1, and TFAM) measured in LV tissue. Data were normalized to the GAPDH expression. On the Y axis, 2-ΔCt ± SEM has been reported, where ΔCt = Ct target gene – Ct GAPDH.

5.6 Ultrastructural analysis of LV myocardium by TEM

TEM images of the LV tissue from CTRL, GTE, and EGCG rat hearts, taken at low and high magnification, are reported in *figure 24*. In all the groups, cardiomyocytes exhibited well-aligned sarcomere striations (*figure 24 A-F*). However, in GTE (*figure 24C-D*) and, to

a less extent, in EGCG (*figure 24E-F*) treated rats, interfibrillar and perinuclear mitochondrial engulfment was evident.

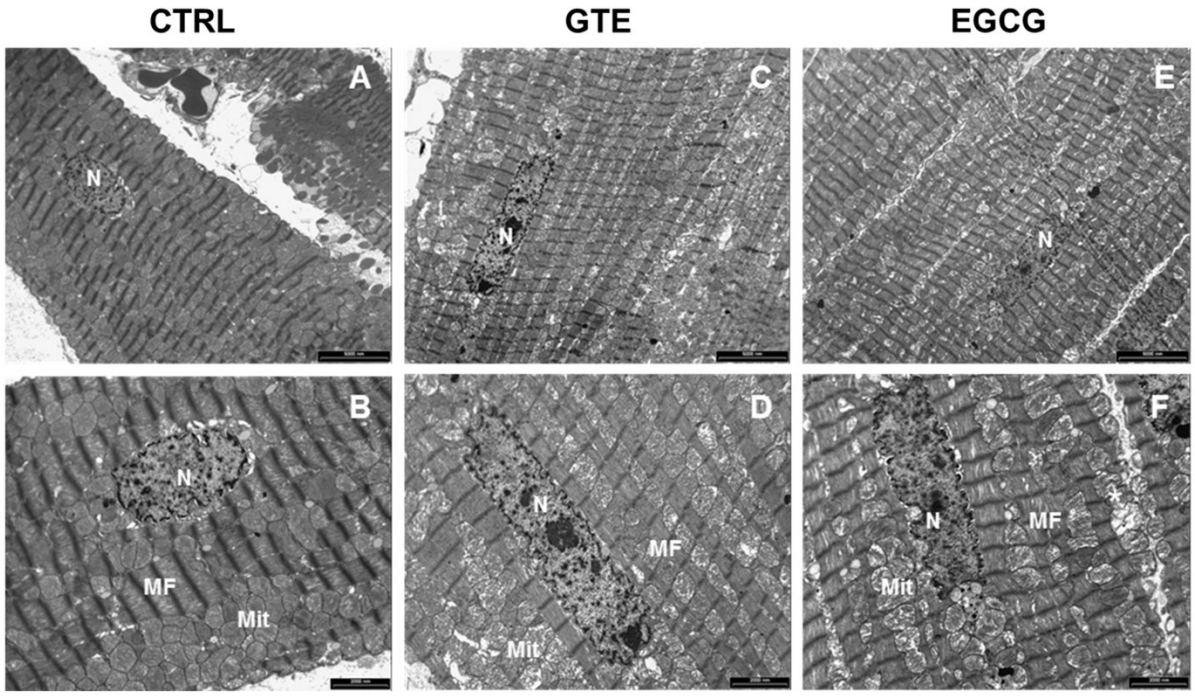

Figure 24. TEM analysis of left ventricular myocardium**.** Representative images of LV tissue from CTRL (**A-B**), GTE (**C-D**), and EGCG (**E-F**) rat hearts, illustrating at different magnification the distribution of mitochondria (Mit) and myofibrils (MF) in cardiomyocytes. N: nucleus. Scale bars=5µm (**A,C,E**); Scale bars=2µm (**B,D,F**).

5.7 Cardiomyocyte mechanics and Ca^{2+} transients

To verify whether the enhanced mitochondrial efficiency induced by GTE and its major component, EGCG, had a functional counterpart in terms of cell mechanical properties, we analysed the cardiomyocyte mechanics and Ca^{2+} transients. The average diastolic sarcomere length (BL, *figure25C)* was similar in all the experimental groups. Conversely, GTE cardiomyocytes exhibited a significant increase in the fraction of shortening (FS, *figure 25D*), in the maximal rate of shortening ($-dl/dt_{max}$, *figure 25E*) and re-lengthening ($+dl/dt_{max}$, *figure 25F*), resulting in a shorter relaxation times measured at 10%, 50%, and 90% of re-lengthening (RL10%, RL50%, RL90%, *figure 25G*) in comparison with both CTRL and EGCG. Consistent with cell motion data, a significant decrease in the time required for cytosolic calcium removal (tau, *figure 25I*) was observed, indicating a faster cytosolic calcium removal. No differences among groups were observed in the amount of Ca^{2+} released from the Sarcoplasmic Reticulum (f/f0, *figure 25H*).

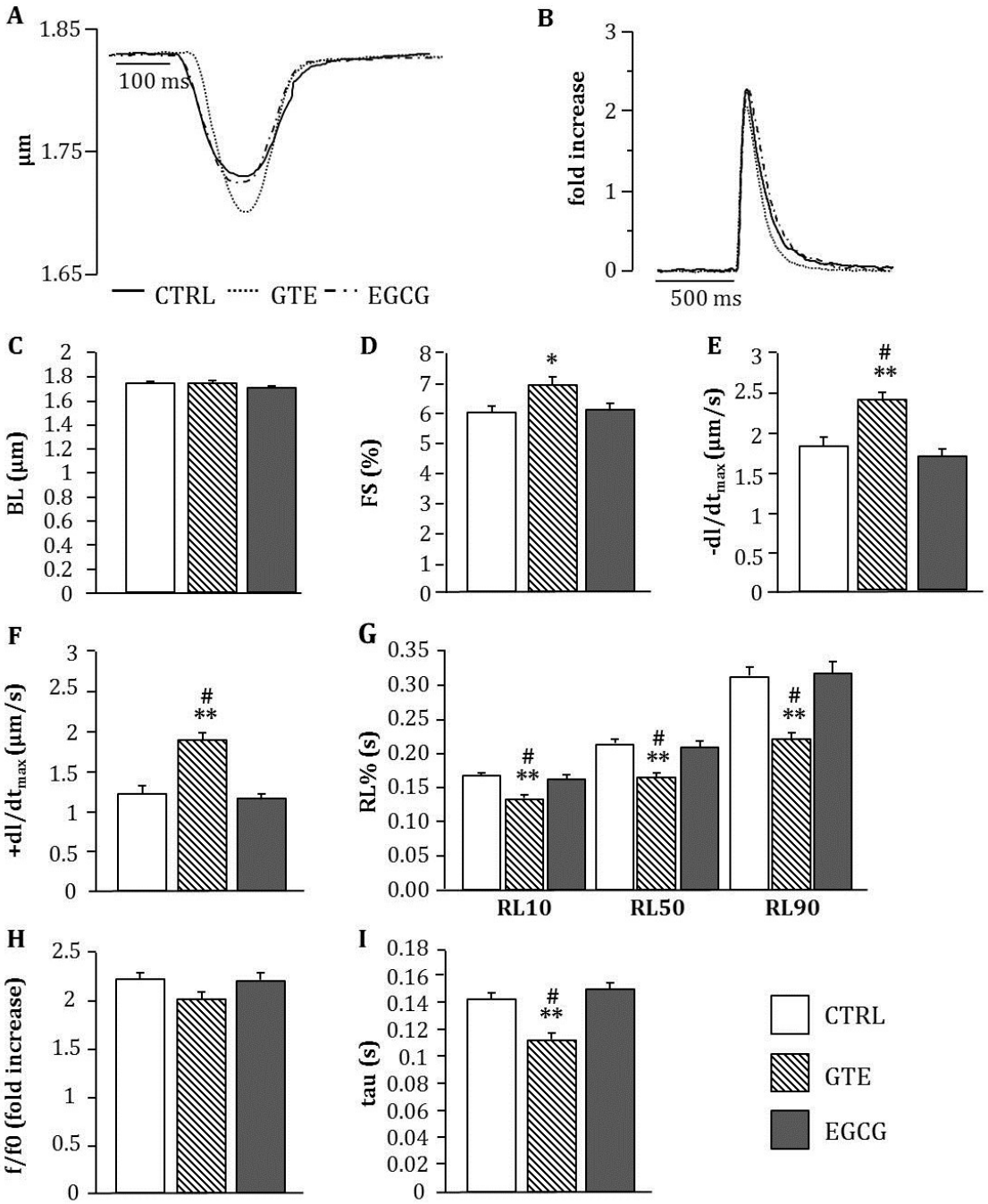

Figure 25. Effects of GTE and EGCG administration on cell mechanics and calcium transients in cardiomyocytes isolated from adult rat hearts. Representative examples of sarcomere shortening (**A**) and corresponding calcium transients (**B**; normalized traces: fold increase) recorded from CTRL (solid line), GTE (dotted line), and EGCG (dashed line) ventricular myocytes. In **C-I** bar graphs means values ± SEM of: mean diastolic sarcomere length (BL; **C**), sarcomere fraction of shortening (FS; **D**), maximal rate of shortening ($-dL/dt_{max}$; **E**), maximal rate of re-lengthening ($+dL/dt_{max}$; **F**), time to 10, 50, and 90% of re-lengthening (RL10%, RL50%, RL90%; **G**), calcium transient amplitude expressed as peak fluorescence normalized to baseline fluorescence (f/f0; **H**), and time constant of the intracellular calcium decay (tau; **I**), measured in CTRL (66 cells), GTE (72 cells) and EGCG (78 cells). * $p<0.05$, ** $p<0.01$ significant differences vs CTRL; # $p<0.01$ significant differences between GTE and EGCG.

5.7 Electrophoresis and western blot analysis of SECA2, PLB, and p-PLB

Western blot analysis showed that the expression levels of SERCA2 were comparable in all experimental group (*figure 26A*). A significant decrease in the total PLB levels (*figure 26B*) was also observed in GTE rats as compared to both EGCG and CTRL rats, while p-PLB expression was comparable among all groups (*figure 26C*). Accordingly, we found a significant increase of both SERCA2/PLB and p-PLB/PLB ratio in GTE samples compared to both EGCG and CTRL (*figure 26D-E*; p> 0.05 vs CTRL and EGCG).

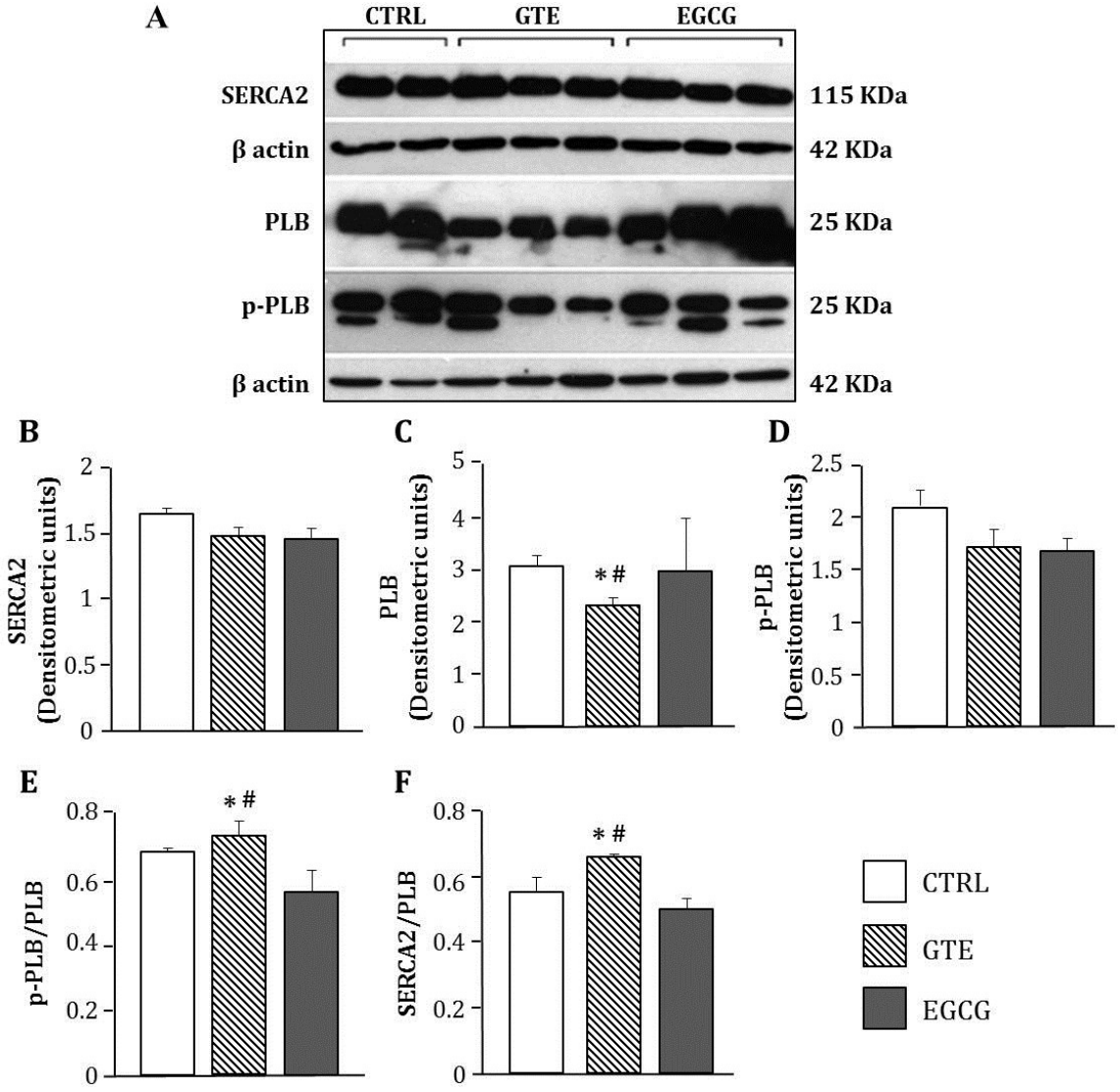

Figure 26. Expression levels of functional proteins by immunoblot assay. **A:** sets of bands related to SERCA, PLB, p-PLB, and β actin expression in CTRL (n=2), GTE (n=3), and EGCG (n=3) left ventricular myocardium. The western blots panels are representative of three different experiments showing similar results. The expression levels of SERCA2 (**B**), PLB (**C**), and p-PLB (**D**) were measured by densitometric analysis and normalized to β-actin. In **E** and **F** are reported p-PLB/PLB and SERCA2/PLB ratio, respectively. Bar graphs show the mean value ± SEM. * p<0.05 significant differences vs CTRL; # p<0.05 significant differences between GTE and EGCG.

6. RESULTS of the EXPERIMENTAL PROTOCOL 2

6.1 Blood glucose levels and body weight

Two days after STZ injection, the blood glucose levels were significantly increased in diabetic rats compared to CTRL (376±15 mg/dl vs 105±4 mg/dl; p<0.01). During the subsequent week, glycaemia increased slightly in untreated as well as GTE-treated diabetic animals, while remained stable in CTRL group until the end of the experimental protocol (*table 6*).

	CTRL	D3	D3_GTE
Day 2	105 ± 4	356 ± 11 **	395 ± 28 **
Day 7	103 ± 4	433 ± 36 **	472 ± 50 **
Day 14	101 ± 5	424 ± 25 **	448 ± 19 **
Day 21	97 ± 5	472 ± 32 **	487 ± 3 **

Table 6. Mean values ± SEM of blood glucose levels (mg/dl) weekly measured in CTRL group and untreated (D3) and GTE-treated (D3_GTE) diabetic animals. ** p<0.01vs CTRL.

A 5% decrease in the body weights were observed during the first two weeks after STZ injection in both treated and untreated diabetic rats. Subsequently, body mass exhibited only negligible changes while in CTRL animals it slightly increased (*table 7*). GTE treatment did not affect both blood glucose level and body weight.

	CTRL	D3	D3_GTE
Day 0	359 ± 9	378± 5	384 ± 7
Day 2	370 ± 9	355 ± 5	364 ± 8
Day 7	379 ± 12	343 ± 5	349 ± 11
Day 14	382 ± 13	332 ± 6 **	335 ± 7 **
Day 21	387 ± 14	331 ± 8 **	336 ± 9 **

Table 7. Mean values ± SEM of body weights (g) weekly measured in CTRL group and untreated (D3) and GTE-treated (D3-GTE) diabetic animals. ** p<0.01vs CTRL.

6.2 Cardiomyocyte mechanics and Ca^{2+} transients

The average diastolic sarcomere length was comparable in all groups (1.74±0.01 μm, 1.70±0.01, 1.70±0.01 in CTRL, D3, and D3_GTE respectively; *figure 27C*). Conversely, contraction/relaxation properties and intracellular calcium dynamics were worsened in unloaded ventricular myocytes isolated from D3 hearts in comparison with CTRL (*figure 27A-I*). Specifically, D3 cardiomyocytes exhibited a significant decrease in the sarcomere fraction of shortening (FS, -17%; *figure 27D*), maximal rate of shortening ($-dL/dt_{max}$, -

27%; *figure 27E*), maximal rate of re-lengthening (+dL/dt_{max}, -31%; *figure 27F*), and time to 90% of re-lengthening (RL90%, -13%; *figure 27G*). The impaired contractility in D3 cells was accompanied by a significant decrease in calcium transient amplitude (f/f0, -18%; *figure 27H*) associated with higher values of the time required for cytosolic calcium clearing (tau, +44%; *figure 27I*). GTE *in vivo* treatment lad to an almost complete recovery of cellular mechanical properties and calcium dynamics (*figure 27A-I)*.

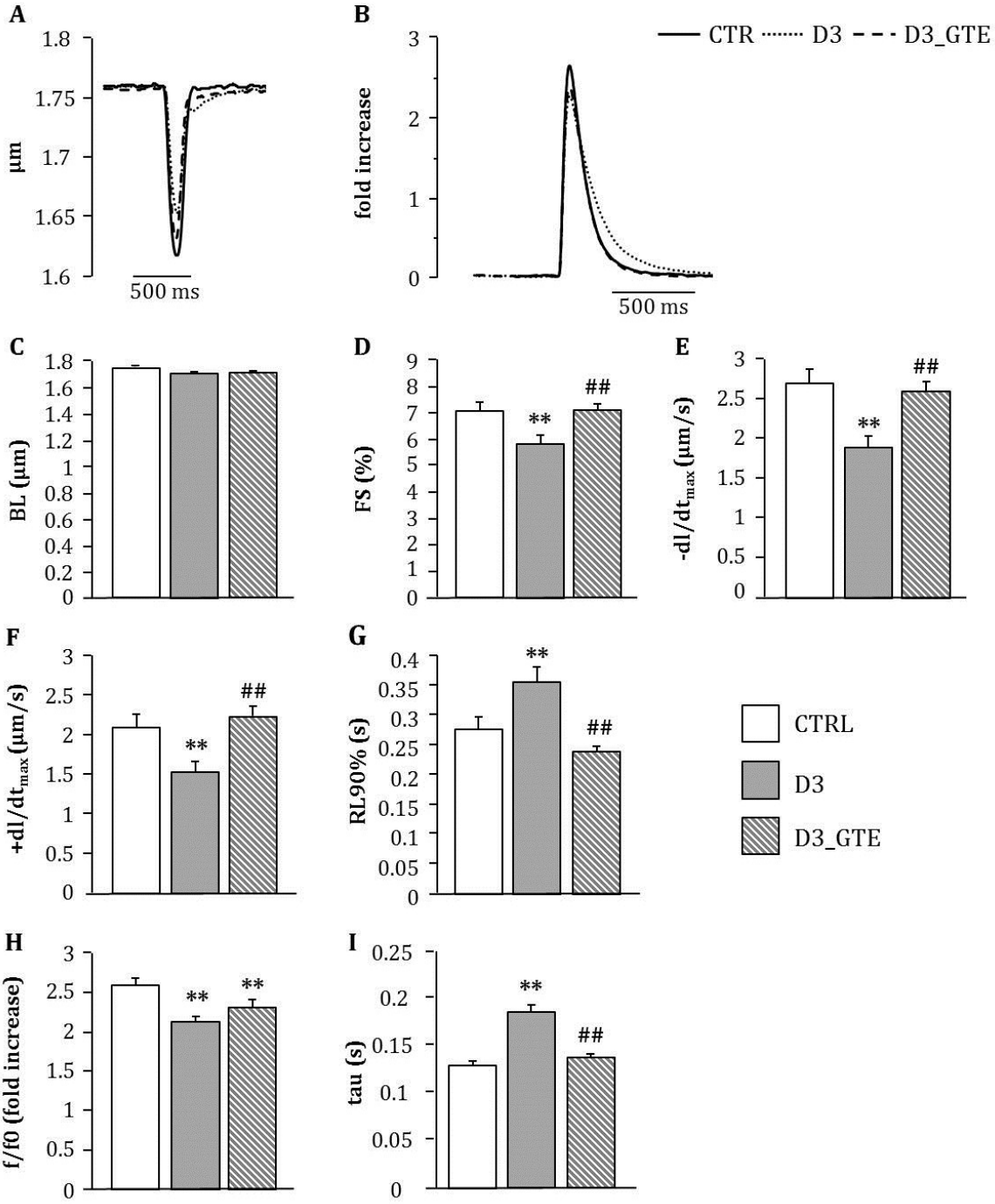

Figure 27. Cell mechanics and calcium transients. Representative examples of sarcomere shortening (**A**) and corresponding calcium transients (**B**; normalized traces: fold increase)

recorded from CTRL (solid line), D3 (dotted line), and D3_GTE (dashed line) ventricular myocytes. In **C–I** bar graphs, means values ± SEM of mean diastolic sarcomere length (BL; **C**), sarcomere fraction of shortening (FS; **D**), maximal rate of shortening ($-dL/dt_{max}$; **E**), maximal rate of re-lengthening ($+dL/dt_{max}$; **F**), time to 90% of re-lengthening (RL90%; **G**), calcium transient amplitude expressed as peak fluorescence normalized to baseline fluorescence (f/f0; **H**), and time constant of the intracellular calcium decay (tau; **I**), measured in CTRL (59 cells), D3 (56 cells), and D3_GTE (55 cells).* $p<0.05$, ** $p<0.01$ significant differences vs CTRL; # $p<0.05$, ## $p<0.01$ significant differences vs D3.

7. DISCUSSION

Green tea is the second most popular drink worldwide [Al Hrooba AM, 2019]. Increased evidence documented a close relationship between the consumption of green tea polyphenols and the risk reduction of several pathological conditions including cancers, metabolic disorders, neurodegenerative pathologies, and cardiovascular disorders [Reygaert WC, 2017]. GTCs have been shown to exert protective effects in different experimental models of heart diseases and age-related ventricular dysfunction [Potenza MA, 2007; Friedrich FW, 2016; Lustosa BB, 2016; Pan B, 2017; Garcia ML, 2017]. However, studies showing potential positive effects on normal heart of *in vivo* long term administration of GTCs, are still lacking.

In the present study we demonstrated that the oral administration of a standardized GTE in healthy rats improve cell mechanical properties and intracellular calcium dynamics by enhancing the SERCA2 activity and cell energy availability, without changes in the expression levels of cardiac ion channels, as measured at mRNA level (L-type Ca^{2+} channel, Na^{+}/Ca^{2+}exchanger, and ryanodine receptor). Specifically, GTE cardiomyocytes, compared with control cells, exhibited a hyperdynamic contractility as demonstrated by an increase in the rate of shortening and re-lengthening, the fraction of shortening, and a more efficient cytosolic calcium removal. Moreover, a faster isovolumic relaxation was observed at organ level. Consistent with these data, we observed a significant increase in the intracellular ATP content in GTE cardiomyocytes as compared with CTRL, as well as in the ratios phosphorylated-PLB/PLB and SERCA2/PLB.

Cardiac muscle contraction is a strictly regulated process which require a very high energetic demand for generating the necessary mechanical force and maintaining cellular homeostasis. In healthy heart the 60-70% of the total ATP, mainly produced from β-oxidation of free FA and oxidative phosphorylation in the mitochondria, is consumed during the sarcomere contractile process while the remaining 30-40% is used for the function of various ion pumps, such as SERCA2, the major regulator of intracellular Ca^{2+} homeostasis [van Opbergen CJM, 2019].

The increased ATP content in GTE cardiomyocytes is in accordance with previous *in vivo* and *in vitro* studies showing that EGCG, the most abundant polyphenol of green tea, regulates: i) mitochondrial function that, in turn, impacts cell bioenergetics (ATP production and anabolism), ii) mitochondrial biogenesis through activation of AMP-activated protein kinase (AMPK), a key metabolic regulator, iii) mitochondrial redox

level, and iv) mitochondrial-related apoptosis [Shi W, 2018]. In line with these evidence, we measured a significant rise in the rate of mitochondria endogenous respiration accompanied by an increased steady-state ATP content in both GTE- and EGCG-treated cardiomyocyte as compared to CTRL cells. This observations led us to hypothesize that the improvement in the cardiomyocyte mitochondrial function could be due to an enhancement in the levels of all the OXPHOS complexes and/or an increase in the mitochondrial mass. Indeed, we documented an increase in the cell respiration rate under state 3 respiratory conditions (or maximal respiration rate) in both GTE and EGCG cardiomyocytes compared to controls, as well as in all OXPHOS complexes level, suggesting an augmented oxidation of the heart energetic substrates, among which fatty acids are the most used. Our data are consistent and support the results of previous studies that documented the beneficial effects of tea catechins in stimulating lipid catabolism and fatty acids β-oxidation [Murase T, 2002].

We also observed a significant enrichment of both Complex I and III in LV tissue of supplemented rats as compared to controls. The lack in the increase of Complexes II and V measured in the LV tissue (at difference to isolated cardiomyocytes) can be explained by the heterogeneity of the myocardium, that comprises fibroblasts and endothelial cells besides cardiomyocytes. The latter occupy the largest fraction of the mammalian heart volume (about 70–80%) [Zhao J, 2019; Zhou P, 2016].

The improved cardiomyocyte bioenergetics did not seem to be explained by changes in the mitochondrial mass, as measured by the citrate synthase activity in isolated cardiomyocytes. This observation was also supported by the analysis of the mtDNA copy number, which is used as a surrogate biomarker of the amount of mitochondria in cells [Costanzini A, 2019], and the expression of genes involved in mitochondrial biogenesis.

The 33% of the ventricular cardiomyocyte volume is occupied by mitochondria, which can be subdivided into two different populations: interfibrillar and subsarcolemmal [van Opbergen CJM, 2019]. Interfibrillar mitochondria run between myofibrils arranged parallel to the long axis of the cardiomyocyte and have mostly tubular orientation of their cristae. Subsarcolemmal mitochondria are clustered below the sarcolemma and display lamellar cristae orientation [Chistiakov DA, 2018].This enforced proximity of mitochondria to sarcomeres throughout the cardiomyocyte provides for a ready and continuous supply of ATP to all components of actin–myosin contractile machinery

[Dorn II GW, 2013]. In particular, as documented by the transmission electron microscopy images, the mitochondria in the GTE- and EGCG-treated cardiomyocytes appeared mainly located at the interfibrillar and perinuclear regions, in the so-called condensed state [Mannella CA, 2006], and are characterized by very dense matrix compartments, suggesting a higher ADP phosphorylation power compared to controls.

Due to the pivotal role of mitochondria in the maintenance of cardiac homeostasis, the increase in the mitochondrial function induced by long-term administration of both GTE and EGCG, should have had a functional counterpart in terms of cardiomyocyte contractile properties that strongly depend on ATP availability [van Opbergen CJM, 2019]. However, we found that only GTE improves cardiomyocyte mechanics and intracellular calcium dynamics, suggesting that additional different intracellular pathways are promoted by the administration of the entire extract, rather than EGCG alone. Indeed, in accordance with our previous data (experimental protocol 1a), GTE cardiomyocytes exhibited a significant increase in the fraction of shortening associated with higher contraction-relaxation rates in comparison with both control and EGCG-treated rats and, consistently, a faster cytosolic calcium removal. By contrast, EGCG given to animals at the equivalent amount that would be in the entirety of GTE did not influence cell contractile/re-lengthening processes.

Additionally, GTE supplementation induced a significant decrease of total PLB levels, leading to an increase of the phosphorylated-PLB/PLB and SERCA2/PLB ratios as compared to both EGCG and CTRL rats. Phospholamban is a key regulator of sarcoplasmic reticulum calcium cycling and cardiac function. The role of PLB was largely elucidated using various genetically altered rodent models or experimental heart failure, as well as by the study of spontaneous mutation of PLB gene in human [MacLennan DH, 2003; Haghighi K, 2014]. Specifically, dephosphorylated PLB inhibits the affinity of the SERCA2 pump for Ca^{2+}, whereas its phosphorylation by PKA, PKC, and CAMKII during β-adrenergic stimulation restores the attenuated SR Ca-ATPase activity, facilitating Ca^{2+}-uptake in the SR and muscle relaxation [MacLennan DH, 2003]. Importantly, an inverse relationship between the relative PLB/SERCA2 ratio and cardiac SR Ca^{2+}-uptake, as well as contractility, has been defined. Studies on PLB knockout mice showed that PLB regulates SERCA2 pump activity by affecting Ca^{2+} affinity of the pump, but not V_{max} of Ca^{2+}-uptake [Periasamy M, 2008]. An increase in PLB to SERCA ratio causes a maximum

inhibition of SERCA pump resulted in depressed cardiac contractility and development of cardiac hypertrophy, whereas a loss of PLB in hearts increases Ca^{2+}-uptake rate and Ca^{2+} store with increased rates of contraction and relaxation with no obvious pathology [Periasamy M, 2008]. This is particularly evident at low frequencies [Meyer M, 1999].
Although we did not investigate the specific intracellular mechanisms leading to the down-regulation of PLB expression in GTE cardiomyocytes, it should be considered that many dietary polyphenols, including green tea catechins, can affect gene expression by epigenetic mechanisms through the modulation of different histone deacetylase activity [Bag A, 2018; Liu L, 2018; Reyes AC, 2019].

In conclusion, we showed that both GTE and EGCG improve cardiomyocyte mitochondrial function by enhancing the OXPHOS complexes levels in healthy rats. However, only *in vivo* administration of GTE positively affected cardiomyocyte mechanics by targeting excitation-contraction key proteins. The lack of effects on cellular mechanics by pure EGCG, given at the same dosage contained in the green tea extract, suggests that the combination of all the catechins contained in the standardized GTE is likely needed to enhance the cardiomyocyte contractile efficiency.

Due to GTE effects on the mitochondrial function and the level of proteins involved in excitation-contraction coupling, we advanced the hypothesis that this standardized GTE might be a valuable adjuvant tool for counteracting the occurrences and/or progression of cardiomyopathies, including diabetic cardiomyopathy, in which mitochondrial dysfunction that reduces energy availability and changes in either the expression or activity of the proteins responsible for the cardiomyocyte contractile efficiency, constitute early pathogenic factors [Gollmer J, 2020; Viola HM, 2019].
For this purpose, in the second part of this study we investigated the ability of early GTE administration to prevent the development of cardiomyocyte contractile dysfunction induced by a short period of hyperglycemia. We used a model of STZ-induced early diabetes widely characterized from a morpho-functional point-of-view. In accordance with our previous studies, showing that 3-weeks of diabetes corresponds to a transitional phase preceding overt DCM phenotype [Savi M, 2016; Savi M, 2017; Bocchi L, 2019], we observed a marked deterioration of cardiomyocyte contractile properties

associated with altered intracellular calcium dynamics, in comparison with controls. The slow Ca^{2+} transient decay and the parallel decrease in the rate of cell re-lengthening is indicative of either impaired re-uptake of Ca^{2+} in the SR or a reduced calcium extrusion through the plasmalemma sodium/calcium exchanger, the two most important players involved in cytosolic calcium clearing [Eisner DA, 2018]. Indeed, several studies on animal models of both type 1 and type 2 diabetes demonstrated that calcium handling machinery was directly impaired as documented by: lower activity levels of SERCA2 and sodium Na^{+}/Ca^{2+} exchanger, impaired ryanodine receptor function, and reduced phospholamban phosphorylation [Borghetti G, 2018]. In addition, in cardiac performance the Ca^{2+} handling is strongly coupled with ATP production which was highly compromised in DCM. Mitochondrial dysfunction and altered myocardial energy metabolism have emerged as important mechanisms implicated in the pathogenesis of DCM. Mechanisms underlying the impairment in mitochondrial function and mitochondrial morphology include oxidative stress, transcriptional and translational alterations of OXPHOS subunit expression, altered energy metabolism-induced mitochondrial uncoupling, impaired mitochondrial Ca^{2+} handling, and altered mitochondrial dynamics and biogenesis [Bugger H, 2014].

The chronic administration of GTE in diabetic rats resulted in an almost complete recovery of cellular mechanical properties and intracellular calcium dynamics, assuming values comparable to controls. In D3_GTE rats, despite a decrease in calcium transient amplitude, we documented a significant improvement in cell contractility likely due to an increase in myofilament calcium sensitivity. Indeed, in a rat model of myocardial infarction was found that GTE supplementation for 18 or 48 days was able to increase the myofilament Ca^{2+} sensitivity, improving left ventricle performance [Hsieh SR, 2009]. Other studies showed a protective role of green tea-derived polyphenols in the myocardium damage induced by acidosis through modulation of the pH-induced change in myofilament Ca^{2+} sensitivity by binding to the cardiac isoform-specific troponin C (cTnC) [Liou YM, 2008]. A recent study also provided evidence that green tea polyphenols regulate myocardial contractility in isolated rat hearts via a PKCε-dependent signalling pathway, without increasing intracellular Ca^{2+} levels [Li D, 2008].

Taken together, our preliminary results suggest that *in vivo* GTE treatment can prevent the occurrence of the early signs of cardiac dysfunction, as measured at cellular levels, in

a rat model of diabetes, after 3 weeks of hyperglycaemia. However, additional studies will be necessary to (i) elucidate the mechanisms by which GTE modulate the expression and/or activity of the main molecules involved in the excitation-contraction processes. and (ii) better evaluate the GTE effects on mitochondrial function and dynamics, widely impaired in DCM.

Our findings, support the idea that green tea dietary polyphenols can constitute new therapeutic adjuvant strategy capable of preventing the initial myocardial damage occurring in the diabetic heart and its progression towards an overt pathological condition.

8. REFERENCES

Actis-Goretta L, Lévèques A, Rein M, et al. Intestinal absorption, metabolism, and excretion of (−)-epicatechin in healthy humans assessed by using an intestinal perfusion technique. *Am J Clin Nutr* 2013; 98, 924–933.

Adhami VM, Siddiqui IA, Sarfaraz S, et al. Effective prostate cancer chemopreventive intervention with green tea polyphenols in the TRAMP model depends on the stage of the disease. *Clin Cancer Res* 2009; 15, 1947-53.

Afzal M, Safer A, Menon M. Green tea polyphenols and their potential role in health and disease. *Inflammopharmacol* 2015; 23, 151–161.

Ahmed S, Marotte H, Kwan K, et al. Epigallocaetchin-3-gallate inhibits IL-6 synthesis and suppresses transsignaling by enhancing soluble gp130 production. *Proc Natl Acad Sci USA* 2008; 105, 14692–14697.

Akhtar N and Haqqi TM. Epigallocatechin-3-gallate suppresses the global interleukin-1beta-induced inflammatory response in human chondrocytes. *Arthritis Res Ther* 2011; 13, 93.

Al Hrooba AM, Abukhalilb MH, Husseinc OE, et al. Pathophysiological mechanisms of diabetic cardiomyopathy and the therapeutic potential of epigallocatechin-3-gallate. *Biomed Pharmacother* 2019; 109, 2155–2172.

Amiot MJ, Riva C, Vinet A. Effects of dietary polyphenols on metabolic syndrome features in humans: A systematic review. *Obes Rev* 2016; 17, 573–586.

Armoskaite V, Ramanauskiene K, Maruska A, et al. The analysis of quality and antioxidant activity of green tea extracts. *J Med Plants Res* 2011; 5, 811–816.

Athithan L, Gulsin GS, McCann GP, et al. Diabetic cardiomyopathy: pathophysiology, theories and evidence to date. *World J Diabetes* 2019; 10, 490-510.

Bag A and Bag N. Tea polyphenols and prevention of epigenetic aberrations in cancer. *J Nat Sci Biol Med* 2018; 9, 2–5.

Banerjee S and Chatterjee J. Efficient extraction strategies of tea (Camellia sinensis) biomolecules. *J Food Sci Technol* 2015; 52, 3158–3168.

Bernatoniene J and Kopustinskiene DM. The role of catechins in cellular responses to oxidative stress. *Molecules* 2018; 23, 965.

Bhardwaj P and Khanna D. Green tea catechins: defensive role in cardiovascular disorders. *Chin J Nat Med* 2013; 11, 345–353.

Bocchi L, Savi M, Naponelli V, et al. Long term oral administration of Theaphenon E improves cardiomyocyte mechanics and calcium dynamics by affecting phospholamban phosphorylation and ATP production. *Cell Physiol Biochem* 2018; 47:1230 1243.

Bocchi L, Motta BM, Savi M, et al. The histone deacetylase inhibitor suberoylanilide hydroxamic acid (SAHA) restores cardiomyocyte contractility in a rat model of early diabetes. *Int J Mol Sci* 2019; 20:1873.

Borghetti G, von Lewinski D, Eaton DE, et al. Diabetic Cardiomyopathy: Current and Future Therapies. Beyond Glycemic Control. *Front Physiol* 2018; 9:1514.

Borradaile NM, Han X, Harp JD, et al. Disruption of endoplasmic reticulum structure and integrity in lipotoxic cell death*. J Lipid Res* 2006; 47, 2726–2737.

Botten D, Fugallo G, Fraternali F, et al. Structural properties of green tea catechins. *J Phys Chem B* 2015; 119, 12860−12867.

Boudina S, Sena S, Theobald H, et al. Mitochondrial energetics in the heart in obesity-related diabetes: direct evidence for increased uncoupled respiration and activation of uncoupling proteins. *Diabetes* 2007; 56, 2457–2466.

Boukhabza M, Hilaly JE, Attiya N, et al. In silico evaluation of the potential antiarrhythmic effect of epigallocatechin-3-gallate on cardiac channelopathies. *Comput Math Methods Med* 2016*;* 7861653.

Bugger H and Abel ED. Mitochondria in the diabetic heart. *Cardiovasc Res* 2010; 88, 229-40.

Bugger H and Abel ED. Molecular mechanisms of diabetic cardiomyopathy. *Diabetologia* 2014; 57, 660–671.

Bursill CA, Abbey M, Roach PD. A green tea extract lowers plasma cholesterol by inhibiting cholesterol synthesis and upregulating the LDL receptor in the cholesterol-fed rabbit. *Atherosclerosis* 2007; 193, 86-93.

Cabrera C, Artacho R, Giménez R. Beneficial effects of green tea: A review. *J Am Coll Nutr* 2006; 25, 79-99.

Cai ZY, Li XM, Liang JP, et al. Bioavailability of tea catechins and its improvement. *Molecules* 2018, 23, 2346.

Cao SY, Zhao CN, Gan RY, et al. Effects and mechanisms of tea and its bioactive compounds for the prevention and treatment of cardiovascular diseases: an updated review. *Antioxidants* 2019; 8, 166.

Chistiakov DA, Shkurat TP, Melnichenko AA, et al. The role of mitochondrial dysfunction in cardiovascular disease: a brief review. *Ann Me*d 2018; 50:121-127.

Chiu J, Farhangkhoee H, Xu BY, et al. PARP mediates structural alterations in diabetic cardiomyopathy*. J Mol Cell Cardiol* 2008; 45, 385–393.

Chong CR, Clarke K, Levelt E. Metabolic remodelling in diabetic cardiomyopathy. *Cardiovasc Res* 2017; 113, 422–430.

Chow HS, Hakim IA, Vining DR, et al. Effects of dosing condition on the oral bioavailability of green tea catechins after single-dose administration of Polyphenon E in healthy individuals. *Clin Cancer Res* 2005; 11, 4627–4633.

Costanzini A, Sgarbi G, Maresca A, et al. Mitochondrial mass assessment in a selected cell line under different metabolic conditions. *Cells* 2019; 8:e1454.

Dai W, Xie D, Lu M, et al. Characterization of white tea metabolome: comparison against green and black tea by a non targeted metabolomics approach. *Food Res Int* 2017; 96, 40–45.

Donà M, Dell'Aica I, Calabrese F, et al. Neutrophil restraint by green tea: inhibition of inflammation, associated angiogenesis, and pulmonary fibrosis. *J Immunol* 2003; 170, 4335–4341.

Dorn II GW. Mitochondrial dynamics in heart disease. *Biochim Biophys Acta* 2013; 1833:233-41.

Droge W. Free radicals in the physiological control of cell function. *Physiol Rev* 2002; 82, 47–95.

Duncan JG. Mitochondrial dysfunction in diabetic cardiomyopathy. *Biochim Biophys Acta* 2011; 1813, 1351–1359.

Eisner DA, Caldwell JL, Kistamás K, et al. Calcium and excitation-contraction coupling in the heart. *Circ Res* 2017; 7;121:181-195.

El Bedoui J, Oak MH, Anglard P, et al. Catechins prevent vascular smooth muscle cell invasion by inhibiting MT1-MMP activity and MMP-2 expression. *Cardiovasc Res* 2005; 67, 317-325.

Eng QY, Punniyakoti VT, Srinivasan R. Molecular understanding of Epigallocatechin gallate (EGCG) in cardiovascular and metabolic diseases. *J Ethnopharmacol* 2018; 210, 296–310.

Erba D, Riso P, Bordoni A, et al. G. Effectiveness of moderate green tea consumption on antioxidative status and plasma lipid profile in humans. *J Nutr Biochem* 2005; 16, 144–149.

Fang MZ, Wang Y, Ai N, et al. Tea polyphenol (–)-epigallocatechin-3-gallate inhibits DNA methyltransferase and reactivates methylation-silenced genes in cancer cell lines. *Cancer Res* 2003; 63, 7563–70.

Farhadi F, Khameneh B, Iranshahi M, et al. M. Antibacterial activity of flavonoids and their structure-activity relationship: An update review. *Phytot Res* 2018; 33, 13–40.

Farhat G, Drummond S, Al-Dujaili EAS. Polyphenols and their role in obesity management: a systematic review of randomized clinical trials. *Phytot Res* 2017; 31, 1005–1018.

Finck BN, Lehman JJ, Leone TC, et al. The cardiac phenotype induced by PPARalpha overexpression mimics that caused by diabetes mellitus. *J Clin Invest* 2002; 109, 121-130.

Finicelli M, Squillaro T, Di Cristo F, et al. Metabolic syndrome, mediterranean diet, and polyphenols: evidence and perspectives. *J Cell Physiol* 2019; 234, 5807–5826.

Frank KF, Bölck B, Erdmann E, et al. Sarcoplasmic reticulum Ca2+-ATPase modulates cardiac contraction and relaxation. *Cardiovasc Res* 2003; 57, 20–7.

Friedrich FW, Flenner F, Nasib M, et al. Epigallocatechin-3-Gallate accelerates relaxation and Ca2+ transient decay and desensitizes myofilaments in healthy and mybpc3-targeted knock-in cardiomyopathic mice. *Front Physiol* 2016; 7:607.

Fuchs F and Grabarek Z. The green tea polyphenol (-)-epigallocatechin-3-gallate inhibits magnesium binding to the C-domain of cardiac troponin C. *J Muscle Res Cell Motil* 2013; 34, 107-113.

Garcia ML, Pontes RB, Nishi EE, et al. The antioxidant effects of green tea reduces blood pressure and sympathoexcitation in an experimental model of hypertension. *Hypertens* 2017; 35, 348-354.

Giacco F and Brownlee M. Oxidative stress and diabetic complications. *Circ Res* 2010; 107, 1058–1070.

Gollmer J, Zirlik A, Bugger H. Mitochondrial Mechanisms in Diabetic Cardiomyopathy. *Diabetes Metab J* 2020; 44:33-53.

Graham HN. Green tea composition, consumption, and polyphenol chemistry. *Prev Med* 1992; 21, 334 350.

Granja A, Pinheiro M, Reis S. Epigallocatechin Gallate nanodelivery systems for cancer therapy. *Nutrients* 2016; 8, 307.

Grigorescu ED, Lacatusu CM, Floria M, et al. Left ventricular diastolic dysfunction in type 2 diabetes—progress and perspectives. *Diagnostics* 2019; 9, 121.

Gupta DA, Bhaskar DJ, Gupta RK. Green tea: a review on its natural anti-oxidant therapy and cariostatic benefits. *Biol Sci Pharm Res* 2014; 2, 8–12.

Haghighi K, Bidwell P, Kranias EG. Phospholamban interactome in cardiac contractility and survival: A new vision of an old friend. *J Mol Cell Cardiol* 2014; 77:160-7.

Halliwell B and Gutteridge JMC. Free radicals in biology and medicine. *OUP Oxford* 2007; 704.

Hong MH, Kim MH, Chang HJ, et al. (-)-Epigallocatechin-3-gallate inhibits monocyte chemotactic protein-1 expression in endothelial cells via blocking NF-kappaB signaling. *Life Sci* 2007; 80, 1957-65.

Hotta Y, Huang L, Muto T, et al. Positive inotropic effect of purified green tea catechin derivative in guinea pig hearts: the measurements of cellular Ca2+ and nitric oxide release. *Eur J Pharmacol* 2006; 552, 123-130.

Hsieh SR, Tsai DC, Chen JY, et al. Green tea extract protects rats against myocardial infarction associated with left anterior descending coronary artery ligation. *Eur J Physiol* 2009; 458:631–642.

Hui K, Feng ZP. Efficient experimental design and analysis of real-time PCR assays. *Channels (Austin)* 2013; 7, 160-170.

Iida Y, Doi T, Nishiwaki RM, et al. (-)-Epigallocatechin gallate selectively inhibits adenosine diphosphate-stimulated human platelet activation: suppression of heat shock protein 27 phosphorylation via p38 mitogen-activated protein kinase. *Mol Med Rep* 2014; 10, 1383–1388.

Islam MA. Cardiovascular effects of green tea catechins: progress and promise. *Recent Pat Cardiovasc Drug Discov* 2012; 7, 88-99.

Jain KS, Kathiravan MK, Somani RS, et al. The biology and chemistry of hyperlipidemia. *Bioorg Med Chem* 2007; 15, 4674.

Jin YR, Im JH, Park ES, et al. Antiplatelet activity of epigallocatechin gallate is mediated by the inhibition of PLC2 phosphorylation, elevation of PGD2 production, and maintaining calcium-ATPase activity*. J Cardiovasc Pharmacol* 2008; 51, 45–54.

Joubert F, Wilding JR, Fortin D, et al. Local energetic regulation of sarcoplasmic and myosin ATPase is differently impaired in rats ith heart failure. *J Physiol* 2008; 586, 5181-5192.

Kabera JN, Semana E, Mussa AR, et al. Plant secondary metabolites: biosynthesis, classification, function and pharmacological properties. *J Pharm Pharmacol* 2014; 2, 377–392.

Kargacin ME, Emmett TL, Kargacin GJ. Epigallocatechin-3-gallate has dual, independent effects on the cardiac sarcoplasmic reticulum/endoplasmic reticulum Ca2+ ATPase. *J Muscle Res Cell Motil* 2011; 32, 89-98.

Kazi DM, Daniel K, Zhong S, et al. Potential molecular targets of tea polyphenols in human tumor cells: significance in cancer prevention. *In vivo* 2002; 16, 397-403.

Khan N and Mukhtar H. Tea and health: studies in humans. *Curr Pharm Des* 2013 ; 19, 6141–6147.

Kim A, Chiu A, Barone MK, et al. Green tea catechins decrease total and low-density lipoprotein cholesterol: a systematic review and meta-analysis. *J Am Diet Assoc* 2011; 111, 1720–1729.

Kim SJ, Amankwah E, Connors S, et al. Safety and chemopreventive effect of Polyphenon E in preventing early and metastatic progression of prostate cancer in TRAMP mice. *Cancer Prev Res (Phila)* 2014; 7, 435-44.

Konig A, Bode C, Bugger H. Diabetes mellitus and myocardial mitochondrial dysfunction: bench to bedside. *Heart Fail Clin* 2012; 8, 551–561.

Koo SI and Noh SK. Green tea as inhibitor of the intestinal absorption of lipids: potential mechanism for its lipid-lowering effect. *J Nutr Biochem* 2007; 18, 179-83.

Krupkova O, Ferguson SJ, Wuertzkozak K. Stability of (-)-epigallocatechin gallate and its activity in liquid formulations and delivery systems. *J Nutr Biochem* 2016; 37, 1–12.

Kuum M, Kaasik A, Joubert F, et al. Energetic state is a strong regulator of sarcoplasmic reticulum Ca2+ loss in cardiac muscle: different efficiencies of different energy sources. *Cardiovasc Res* 2009; 83, 89-96.

Lagha AB, Haas B, Grenier D. Tea polyphenols inhibit the growth and virulence properties of Fusobacterium nucleatum. *Sci Rep* 2017; 7, 44815.

Lambert JD and Elias RJ. The antioxidant and pro-oxidant activities of green tea polyphenols: a role in a cancer prevention. *Arch Biochem Biophys* 2010; 501, 65–72.

Lau SO, Georgousopoulou EN, Kellett J, et al. The effect of dietary supplementation of green tea catechins on cardiovascular disease risk markers in humans: a systematic review of clinical trials, *Beverages* 2016; 2, 16.

Lee DH, Kim YJ, Kim HH, et al. Inhibitory effects of epigallocatechin-3-gallate on microsomal cyclooxygenase-1 activity in platelets. *Biomol Ther* 2013; 21, 54–59.

Lee KM, Yeo M, Choue JS, et al. Protective mechanism of epigallocatechin-3-gallate against Helicobocter pylori-induced gastric epithelial cytotoxicity via the blockage of TLR-4 signaling. *Helicobacter* 2004; 9, 632–642.

Levelt E, Mahmod M, Piechnik SK, et al. Relationship between left ventricular structural and metabolic remodeling in type 2 diabetes. *Diabetes* 2016; 65, 44-52.

Li D, Yang C, Chen Y, et al. Identification of a PKCε-dependent regulation of myocardial contraction by epicatechin-3-gallate. *Am J Physiol Heart Circ Physiol* 2008; 294: H345–H353.

Liou YM, Kuo SC, Hsieh SR. Differential effects of a green tea-derived polyphenol (−)-epigallocatechin-3-gallate on the acidosis-induced decrease in the Ca2+ sensitivity of cardiac and skeletal muscle. *Pflugers Arch* 2008; 456:787–800.

Liu L, Zhao W, Liu J, et al. Epigallocatechin-3 gallate prevents pressure overloadinduced heart failure by up-regulating SERCA2a via histone acetylation modification in mice. *PLoS One* 2018; 13: 0205123.

Liu Q, Wang S, Cai L. Diabetic cardiomyopathy and its mechanisms: role of oxidative stress and damage. *J Diabetes Investig* 2014; 5, 623–634.

Lorenz M, Hellige N, Rieder P, et al. Positive inotropic effects of epigallocatechin-3-gallate (EGCG) involve activation of Na+/H+ and Na+/Ca2+ exchangers. *Eur J Heart Fail* 2008; 10, 439-445.

Ludwig A, Lorenz M, Grimbo N, et al. The tea flavonoid epigallocatechin-3-gallate reduces cytokine-induced VCAM-1 expression and monocyte adhesion to endothelial cells. *Biochem Biophys Res Commun* 2004; 316, 659-665.

Lustosa BB, Polegato B, Minicucci M, et al. Green tea (Cammellia sinensis) attenuates ventricular remodeling after experimental myocardial infarction. *Int J Cardiol* 2016; 225, 147–153.

MacLennan DH, Kranias EG. Phospholamban: a crucial regulator of cardiac contractility. *Nat Rev Mol Cell Biol* 2003; 4: 566–577.

Manach C, Scalbert A, Morand C, et al. Polyphenols: food sources and bioavailability. *Am J Clin Nutr* 2004; 79, 727–747.

Mannella CA. Structure and dynamics of the mitochondrial inner membrane cristae. *Biochim Biophys Acta* 2006; 1763: 542–548.

Mazumder PK, O'Neill BT, Roberts MW, et al. Impaired cardiac efficiency and increased fatty acid oxidation in insulin-resistant ob/ob mouse hearts. *Diabetes* 2004; 53, 2366–2374.

Metodiewa D, Kochman A, Karolczak S. Evidence for antiradical and antioxidant properties of four biologically active N, N, diethylaminoethyl ethers of flavanone oximes: a comparison with natural polyphenolic flavonoid (rutin) action. *Biochem Mol Biol Int* 1997; 41, 1067–1075.

Meyer M, Bluhm WF, He H, et al. Phospholamban-to-SERCA2 ratio controls the force-frequency relationship. *Am J Physiol* 1999; 276: H779-785.

Murase, T, Nagasawa A, Suzuki J, et al. Beneficial effects of tea catechins on diet-induced obesity: stimulation of lipid catabolism in the liver. *Int J Obes Relat Metab Disord* 2002, 26, 1459-1464.

Musial C, Kuban-Jankowska A, Gorska-Ponikowska M. Beneficial properties of green tea catechins. *Int J Mol Sci* 2020; 21, 1744.

Nagao T, Hase T, Tokimitsu I. A green tea extract high in catechins reduces body fat and cardiovascular risks in humans. *Obesity (Silver Spring)* 2007; 15, 1473–1483.

Nakachi K, Matsuyama S, Miyake S, et al. Preventive effects of drinking green tea on cancer and cardiovascular disease: epidemiological evidence for multiple targeting prevention. *Biofactors* 2000; 13, 49–54.

Nelson RH. Hyperlipidemia as a risk factor for cardiovascular disease. *Prim Care* 2013; 40, 195–211.

Nicholson JK, Holmes E, Kinross J, et al. Host-gut microbiota metabolic interactions. *Science* 2012; 336, 1262-1267.

Nicklas JA, Brooks EM, Hunter TC, et al. Development of a quantitative PCR (TaqMan) assay for relative mitochondrial DNA copy number and the common mitochondrial DNA deletion in the rat. *Environ Mol Mutagen* 2004; 44, 313-20.

Ostrander DB, Sparagna GC, Amoscato AA, et al. Decreased cardiolipin synthesis corresponds with cytochrome c release in palmitate-induced cardiomyocyte apoptosis. *J Biol Chem* 2001; 276, 38061–38067.

Pan B, Quan J, Liu L, et al. Epigallocatechin gallate reverses cTnI-low expression-induced age-related heart diastolic dysfunction through histone acetylation modification. *J Cell Mol Med* 2017; 21, 2481-2490.

Panche AN, Diwan AD, Chandra SR. Flavonoids: An overview. *J Nutritional Sci* 2016; 5, 47.

Pastoriza S, Mesías M, Cabrera C, et al. Healthy properties of green and white teas: an update. *Food Funct* 2017; 8, 2650-2662.

Pattison JS, Waggoner JR, James J, et al. Phospholamban overexpression in transgenic rabbits. *Transgenic Res* 2008; 17, 157–170.

Periasamy M, Bhupathy P, Babu GJ. Regulation of sarcoplasmic reticulum Ca2+ ATPase pump expression and its relevance to cardiac muscle physiology and pathology. *Cardiovasc Res* 2008; 15;77:265-73.

Potenza MA, Marasciulo FL, Tarquinio M, et al. EGCG, a green tea polyphenol, improves endothelial function and insulin sensitivity, reduces blood pressure, and protects against myocardial I/R injury in SHR. *Am J Physiol Endocrinol Metab* 2007; 292, 1378–87.

Prasad AM, Inesi G. Silencing calcineurin A subunit reduces SERCA2 expression in cardiac myocytes. *Am J Physiol Heart Circ Physiol* 2011; 300:H173-H180.

Pullikotil P, Chen H, Muniyappa R, et al. Epigallocatechin gallate induces expression of heme oxygenase-1 in endothelial cells via p38 MAPK and Nrf-2 that suppresses proinflammatory actions of TNF-alpha. *J Nutr Biochem* 2011; 23, 1134-45.

Rasouli H, Bagher Hosseini Ghazvini SM, Khodarahm R. Chapter 3: Therapeutic potentials of the most studied flavonoids: Highlighting antibacterial and antidiabetic functionalities. *Studies in Natural Products Chemistry* 2018; 60, 85–118.

Rehman H, Krishnasamy Y, Haque K, et al. Green tea polyphenols stimulate mitochondrial biogenesis and improve renal function after chronic cyclosporin a treatment in rats. *PLoS One* 2014; 8, e65029.

Reyes AC, López-González JS, Flores MM, et al. Dietary Compounds as Epigenetic Modulating Agents in Cancer. *Front Genet* 2019; 1;10:79.

Reygaert WC. The antimicrobial possibilities of green tea. *Front Microbiol* 2014; 5, 434.

Reygaert WC. An update on the health benefits of green tea. *Beverages* 2017; 3, 6.

Reygaert WC. Green tea catechins: their use in treating and preventing infectious diseases. *Biomed Res Int* 2018; 9105261.

Roshanak S, Rahimmalek M, Goli SAH. Evaluation of seven different drying treatments in respect to total flavonoid, phenolic, vitamin C content, chlorophyll, antioxidant activity and color of green tea (Camellia sinensis or C. assamica) leaves. *J Food Sci Technol* 2016; 53, 721–729.

Santangelo C, VarÏ R, Scazzocchio B, et al. Polyphenols, intracellular signalling and inflammation. *Ann Ist Super Sanita* 2007; 43, 394–405.

Santos CN, Gomes A, Oudot C, et al. Pure polyphenols applications for cardiac health and disease. *Curr Pharm Des* 2018; 24:2137-2156.

Savi M, Bocchi L, Sala R, et al. Parenchymal and stromal cells contribute to pro-inflammatory myocardial environment at early stages of diabetes: protective role of resveratrol. *Nutrients* 2016; 8, 729.

Savi M, Bocchi L, Mena P, et al. In vivo administration of urolithin A and B prevents the occurence of cardiac dysfunction in streptozotocin-induced diabetic rats. *Cardiovasc Diabetol* 2017; 16:80.

Serafini M, Del Rio D, Yao DN, et al. Health benefits of tea. *In Herbal Medicine: Biomolecular, and Clinical Aspects, 2nd ed; Benzie IFF,Wachtel-Galor S, Eds; CRC Press: Boca Raton, FL, USA* 2011; 239–262.

Shang Y, Zhang X, Leng W, et al. Assessment of diabetic cardiomyopathy by cardiovascular magnetic resonance T1 mapping: correlation with left-ventricular diastolic dysfunction and diabetic duration. *J Diabetes Res* 2017; 9584278.

Shi W, Li L, Ding, Yang K, et al. The critical role of epigallocatechin gallate in regulating mitochondrial metabolism. *Future Med Chem* 2018; 10, 795–809.

Son DJ, Cho MR, Jin YR, et al. Antiplatelet effect of green tea catechins: a possible mechanism through arachidonic acid pathway. *Prostaglandins Leukot Essent Fatty Acids* 2004; 71, 25–31.

Spina M, Cuccioloni M, Mozzicafreddo M, et al. Mechanism of inhibition of wt-dihydrofolate reductase from E. coli by tea epigallocatechin-gallate. *Proteins* 2008; 72, 240–251.

Srinivasan M and Lahiri DK. Significance of NF-kappaB as pivotal therapeutic agent in the neurodegenerative pathologies of Alzheimer's disease and multiple sclerosis. *Expert Opin Ther Targets* 2015; 19, 471–487.

Stalmach A, Mullen W, Steiling H, et al. Absorption, metabolism, and excretion of green tea flavan-3-ols in humans with an ileostomy. *Mol Nutr Food Res* 2010; 54, 323–334.

Stilli D, Lagrasta C, Berni R, et al. Preservation of ventricular performance at early stages of diabetic cardiomyopathy involves changes in myocyte size, number and intercellular coupling. *Basic Res Cardiol* 2007; 102, 488-99.

Subramani C and Natesh RK. Molecular mechanisms and biological implications of green tea polyphenol, (-)-epigallocatechin-3-gallate. *Int J Pharm Biosci Technol* 2013; 1, 54–63.

Sucato V, Novo G, Evola S, et al. Coronary microvascular dysfunction in patients with diabetes, hypertension and metabolic syndrome. *Int J Cardiol* 2015; 186, 96-97.

Suzuki E, Yorifuji T, Takao S, et al. Green tea consumption and mortality among Japanese elderly people: the prospective Shizuoka elderly cohort. *Ann Epidemiol* 2009; 19, 732-9.

Suzuki-Sugihara N, Kishimoto Y, Saita E, et al. Green tea catechins prevent low-density lipoprotein oxidation via their accumulation in low-density lipoprotein particles in humans. *Nutr Res* 2016; 36, 16–23.

Tang WJ, Hu CP, Chen MF, et al. Epigallocatechin gallate preserves endothelial function by reducing the endogenous nitric oxide synthase inhibitor level. *Can J Physiol Pharmacol* 2006; 84, 163-171.

Tungmunnithum D, Thongboonyou A, Pholboon A, et al. Flavonoids and other phenolic compounds from medicinal plants for pharmaceutical and medical aspects: an overview. *Medicine* 2018; 5, 93.

Valian N, Ahmadiani A, Dargahi L. Escalating methamphetamine regimen induces compensatory mechanisms, mitochondrial biogenesis, and GDNF expression, in substantia nigra. *J Cell Biochem* 2017; 118, 1369-78.

van Opbergen CJM, den Braven L, Delmar M, et al. Mitochondrial Dysfunction as Substrate for Arrhythmogenic Cardiomyopathy: A Search for New Disease Mechanisms. *Front Physiol* 2019; 10:1496.

Varga ZV, Giricz Z, Liaudet L, et al. Interplay of oxidative, nitrosative/nitrative stress, inflammation, cell death and autophagy in diabetic cardiomyopathy. *Biochim Biophys Acta* 2015; 1852, 232–242.

Vilella R, Sgarbi G, Naponelli V, et al. Effects of Standardized Green Tea Extract and Its Main Component, EGCG, on Mitochondrial Function and Contractile Performance of Healthy Rat Cardiomyocytes. Nutrients 2020; 12:E2949.

Viola HM and Hool LC. Impaired calcium handling and mitochondrial metabolic dysfunction as early markers of hypertrophic cardiomyopathy. *Arch Biochem Biophys* 2019; 665, 166-174.

Walker EH, Pacold ME, Perisic O, et al. Structural determinations of phosphoinositide 3-kinase inhibition by wortmannin, LY294002, quercetin, myricetin, and staurosporine. *Mol Cell* 2000; 6, 909–919.

Wang H, Provan GJ, Helliwell K. Tea flavonoids: their functions, utilisation and analysis. *Trends Food Sci Technol* 2000; 11, 152–160.

Wang Y and Ma S. Recent advances in inhibitors of bacterial fatty acid synthesis type II (FASII) system enzymes as potential antibacterial agents. *Chem Med Chem* 2013; 8, 1589–1608.

Wende AR, Symons JD, Abel ED. Mechanisms of lipotoxicity in the cardiovascular system. *Curr Hypertens Rep* 2012; 14, 517–531.

Won SM, Park YH, Kim HJ, Park KM, Lee WJ. Catechins inhibit angiotensin II-induced vascular smooth muscle cell proliferation *via* mitogen-activated protein kinase pathway. *Exp Mol Med* 2006; 38, 525-534.

Woodwarda KA, Draijerb R, Thijssena DHJ, et al. Polyphenols and microvascular function in humans: a systematic review. *Curr Pharm Des* 2018; 24:203-226.

Xing L, Zhang H, Qi R, et al. Recent advances in the understanding of the health benefits and molecular mechanisms associated with green tea polyphenols. *J Agric Food Chem* 2019; 67, 1029−1043.

Yamagata K. Protective effect of epigallocatechin gallate on endothelial disorders in atherosclerosis. *J Cardiovasc Pharmacol* 2019; 75, 292-298.

Yamagishi SI, Nakamura N, Suematsu M, et al. Advanced glycation end products: a molecular target for vascular complications in diabetes. *Mol Med* 2015; 21, S32-40.

Yang J, Han Y, Sun H, et al. (−)-Epigallocatechin gallate suppresses proliferation of vascular smooth muscle cells induced by high glucose by inhibition of PKC and ERK1/2 signalings. *J Agric Food Chem* 2011; 59, 11483-11490.

Ye Y, Yan J, Cui J, et al. Dynamic changes in amino acids, catechins, caffeine and gallic acid in green tea during withering. *J Food Compos Anal* 2018; 66, 98–108.

Yousaf S, Butt MS, Suleria HA, et al. The role of green tea extract and powder in mitigating metabolic syndromes with special reference to hyperglycemia and hypercholesterolemia. *Food Function* 2014; 5, 545–556

Yun HJ, Yoo WH, Han MK, et al. Epigallocatechin-3-gallate suppresses TNF-*a*-induced production of MMP-1 and -3 in rheumatoid arthritis synovial fibroblasts. *Rheumatol Int* 2008; 29, 23–29.

Zhang C, Suen CLC, Yang C, et al. Antioxidant capacity and major polyphenol composition of teas as affected by geographical location, plantation elevation and leaf grade. *Food Chem* 2018, 244, 109–119.

Zhang H, Tang B, Row K. Extraction of catechin compounds from green tea with a new green solvent. *Chem Res Chinese U* 2014; 30, 37–41.

Zhang H and Tsao, R. Dietary polyphenols, oxidative stress andantioxidant and anti-inflammatory effects. *Curr Opin Food Sci* 2016; 8, 33–42.

Zhang Z, Li G, Szeto SS, et al. Examining the neuroprotective effects of protocatechuic acid and chrysin on in vitra and in vivo models of Parkinson disease. *Free Radic Biol Med* 2015; 84, 331–343.

Zhao J, Gao JL, Zhu JX, et al. The different response of cardiomyocytes and cardiac fibroblasts to mitochondria inhibition and the underlying role of STAT3. *Basic Res Cardiol* 2019; 114: 12.

Zhou P, Pu WT. Recounting cardiac cellular composition. *Circ Res* 2016; 118: 368-370.

Zuo X, Tian C, Zhao N, et al. Tea polyphenols alleviate high fat and high glucose-induced endothelial hyperpermeability by attenuating ROS production via NADPH oxidase pathway. *BMC Res Notes* 2014; 7, 120.